The Whakamaru Magmatic System (Taupō Volcanic Zone, New Zealand), Part 2: Evidence from ignimbrite deposits for the pre-eruptive distribution of melt-dominated magma and magma mushes

Harmon, Lydia J, *ljharmo1@asu.edu, Department of Earth & Environmental Sciences, Vanderbilt University, 2301 Vanderbilt Place, Nashville, TN 37235, USA and School of Earth and Space Exploration, Arizona State University, 781 Terrace Mall, Tempe, AZ 85287, USA

Smithies, Sarah L, School of Earth and Environment, University of Canterbury, Private Bag 4800, Christchurch 8140, New Zealand. 0000-0002-7734-2952

Gualda, Guilherme A R, Department of Earth & Environmental Sciences, Vanderbilt University, 2301 Vanderbilt Place, Nashville, TN 37235, USA. 0000-0003-0720-2679

Gravley, Darren M, School of Earth and Environment, University of Canterbury, Private Bag 4800, Christchurch 8140, New Zealand. 0000-0003-4451-9210

ABSTRACT

The complex volcanology and petrology of the Whakamaru volcanic deposits in Aotearoa New Zealand have thus far obscured the number of eruptive phases and the relative timing of these eruption(s). We investigate pumice clasts from multiple localities to elucidate the relative timing of the eruptions, with a focus on the pre-eruptive conditions of the melt-dominated magma bodies that fed the Whakamaru eruptions and on the mushes from which these magmas were extracted. Paired whole-rock and glass compositions confirm four magma types erupted during the Whakamaru eruptions (types A, B, C, D; originally identified by Brown *et al.*, 1998). Using the glass compositions of the pumice clasts, we calculate pre-eruptive storage temperatures (using zircon saturation geothermometry) and pressures (using rhyolite-MELTS geobarometry). Using matching whole-rock compositions from a subset of pumice clasts, we calculate extraction pressures from magma mush (also using rhyolite-MELTS geobarometry). Pre-eruptive storage pressures estimate the depths where melt-dominated magma bodies were located prior to eruption; extraction pressures, in contrast, estimate the depths at which melt was extracted from magma mush to form melt-dominated magma bodies at shallower levels of the crust. Magmas were stored at shallow depths (~50-150 MPa) prior to eruption. Extraction pressures for types B and C are well constrained to 155-355 MPa (with an assemblage including plagioclase and quartz). Extraction pressures for types A and D depend on oxygen fugacity (f_{O2}), as the extraction assemblage includes plagioclase and orthopyroxene (170-290 MPa for ΔNNO = 0 to +0.5 and 290-360 MPa for ΔNNO = +1 to +1.5). The four magma types likely represent independent magma bodies, with these melt-dominated magma bodies stored shallower than and separate from the mush. At least two different magma subsystems fed the Whakamaru eruptions – one subsystem sourced the type A and type D magmas, while the other sourced the type B and type C magmas. The distribution of magma types recorded in the ignimbrite deposits and in the correlated tephras (Harmon *et al.*, 2024) reveal the sequence of eruption for the four different mappable ignimbrites. The ignimbrites to the east of the caldera (Rangitaiki ± Te Whaiti) erupted before the Whakamaru ignimbrite (*sensu stricto*) to the west of the caldera. The youngest Whakamaru ignimbrite eruptions likely deposited to the northwest of the caldera contemporaneously with the Manunui ignimbrite to the west of the caldera. The combination of petrological data from the ignimbrites and associated tephras suggest a complex system that included laterally juxtaposed melt-dominated magmas as well as laterally juxtaposed magma mushes that spanned much of the shallow crust, but with regions in which magma appeared in low concentration or was entirely absent. This complex pre-eruptive architecture probably contributed to the complex eruptive patterns observed for the Whakamaru eruptions.

KEY WORDS

Whakamaru group ignimbrites; Whakamaru ignimbrite; Rangitaiki ignimbrite; Manunui ignimbrite; Te Whaiti ignimbrite; Taupō Volcanic Zone; magma storage; geobarometry; magma extraction; glass geochemistry; pumice

INTRODUCTION

Large, explosive volcanic eruptions demonstrate that the crust must create and accommodate large volumes of melt-dominated magma prior to eruption. Substantial advances have been made to understand the pre-eruptive conditions of the melt-dominated magma bodies that feed such eruptions (Cashman & Giordano, 2014), including crystallization timescales (Simon and Reid, 2005; Charlier *et al.*, 2008; Druitt *et al.*, 2012; Allan *et al.*, 2013; Barboni and Schoene, 2014; Chamberlain *et al.*, 2014; Cooper and Kent, 2014; Pamukçu *et al.*, 2015a; Gualda and Sutton, 2016; Fabbro *et al.*, 2017; Reid and Vazquez, 2017; Shamloo and Till, 2019; Chakraborty and Dohmen, 2022); storage pressures (Blundy and Cashman, 2008; Hansteen and Klügel, 2008; Putirka, 2008; Ridolfi *et al.*, 2010; Gualda and Ghiorso, 2013a; Bégué *et al.*, 2014a; Bachmann and Huber, 2016; Gualda *et al.*, 2018; Pitcher *et al.*, 2021; Pelullo *et al.*, 2022); volatile content (Moore *et al.*, 1998; Papale *et al.*, 2006; Ghiorso and Gualda, 2015; Waters and Lange, 2015; Iacovino *et al.*, 2021; Wieser *et al.*, 2022); and oxygen fugacity (f_{O2}) conditions (McCanta *et al.*, 2004; Kelley and Cottrell, 2009; Ulmer *et al.*, 2018; Pitcher *et al.*, 2021; Ghiorso *et al.*, 2023). These eruptions have a variety of possible pre-eruptive storage configurations as they can erupt from one magma body, as in the 'mush' model (Hildreth, 1979; Bachmann and Bergantz, 2004, 2008; Hildreth and Wilson, 2007; Deering *et al.*, 2011; Pamukçu *et al.*, 2013; Chamberlain *et al.*, 2015; Foley *et al.*, 2020) or from multiple melt-dominated magma bodies (Gravley *et al.*, 2007; Cooper *et al.*, 2012; Gualda and Ghiorso, 2013b; Bégué *et al.*, 2014a; Cashman and Giordano, 2014; Swallow *et al.*, 2018; Pearce *et al.*, 2020). This precludes a one-model-fits-all approach to understanding melt-dominated magma bodies.

It is recognized that magmatism is a crustal-scale phenomenon (Annen *et al.*, 2015; Cashman *et al.*, 2017; Karakas *et al.*, 2017; Weinberg *et al.*, 2021; Hilley *et al.*, 2022), such that there is increasing interest in constraining the depths from which melt-dominated magmas (defined below) are extracted from magma mush (Gualda *et al.*, 2019; Blundy, 2022). In contrast to the melt-dominated magma bodies, the bodies of magma mush from which melt-dominated magmas are extracted can be much longer lived and they can be much more widespread in their vertical distribution in the crust (Annen *et al.*, 2015; Reid and Vazquez, 2017; Gualda *et al.*, 2019; Sparks *et al.*, 2019; Blundy, 2022; Giordano and Caricchi, 2022).

Extraction pressures (Gualda *et al.*, 2019) allow us to use erupted volcanic rocks to derive important information on the location of magma mushes in the crust (see also Pamukçu et al., 2021; Pitcher et al., 2021; Smithies et al., 2023). Understanding how the crust can produce melt-dominated magma from the magma mush is paramount in elucidating the dynamics of large magmatic systems.

The Taupō Volcanic Zone (TVZ) Whakamaru group eruptions expelled >2000 km^3 of melt-dominated, rhyolitic magma from a large magmatic system (Wilson *et al.*, 1986; Brown *et al.*, 1998; Matthews *et al.*, 2012; Downs *et al.*, 2014). The eruptions kicked off a period of high volcanic activity (i.e., an ignimbrite flare-up, Gravley et al., 2016), which led to the eruption of – in addition to the Whakamaru group itself – six caldera-forming eruptions over the ensuing ~100 ka (see also Gualda *et al.*, 2018; Smithies *et al.*, 2023). The Whakamaru group ignimbrites are known to have erupted pumice of multiple compositions (Brown *et al.*, 1998; Harmon *et al.*, 2024), indicating the presence of multiple magma types in the magmatic system.

Here, we investigate the pre-eruptive magmatic conditions (temperature, pressure, and composition) for melt-dominated magma bodies, as well as the extraction conditions for magma mush bodies from the Whakamaru group eruptions to constrain the configuration of the upper crustal reservoir that sourced the largest eruption in young TVZ history. The goal is to understand what the crust looks like prior to very large to supereruptions (VEI >6).

The terminology we use here follows Smithies *et al.* (2023) and Harmon *et al.* (2024), demonstrated schematically in Figure 1. A ***magma body*** is a parcel of magma that is in contact with rocks or other magmas, with clear boundaries. We define melt-dominated magma bodies and magma mush bodies. A ***melt-dominated magma body*** is composed of crystal-poor magma that typically has a suspension of crystals (and possibly bubbles). It can be erupted imminently. Melt-dominated magma is extracted from the ***magma mush body***. A ***magma mush body*** is composed of crystal-rich magma that contains a framework of touching crystals with interstitial melt (± bubbles). The magma mush is unlikely to be readily erupted. A ***magma type*** is a compositionally and texturally homogeneous group of magmas where a given magma type may be characteristic of a magma body, or it may be present in multiple magma bodies. The ***magma system*** includes all magma bodies through the lifetime of the system. We follow Gualda *et al.* (2019) and distinguish ***contiguous magma bodies***, in which melt-dominated magma is in direct contact with magma mush, as typically invoked in the 'mush' model (Bachmann and Bergantz, 2004, 2008; Hildreth, 2004), and ***non-contiguous magma bodies***, in which melt-dominated magma is detached from the magma mush body from which it was extracted and has migrated to a shallower storage zone (see Figure 1).

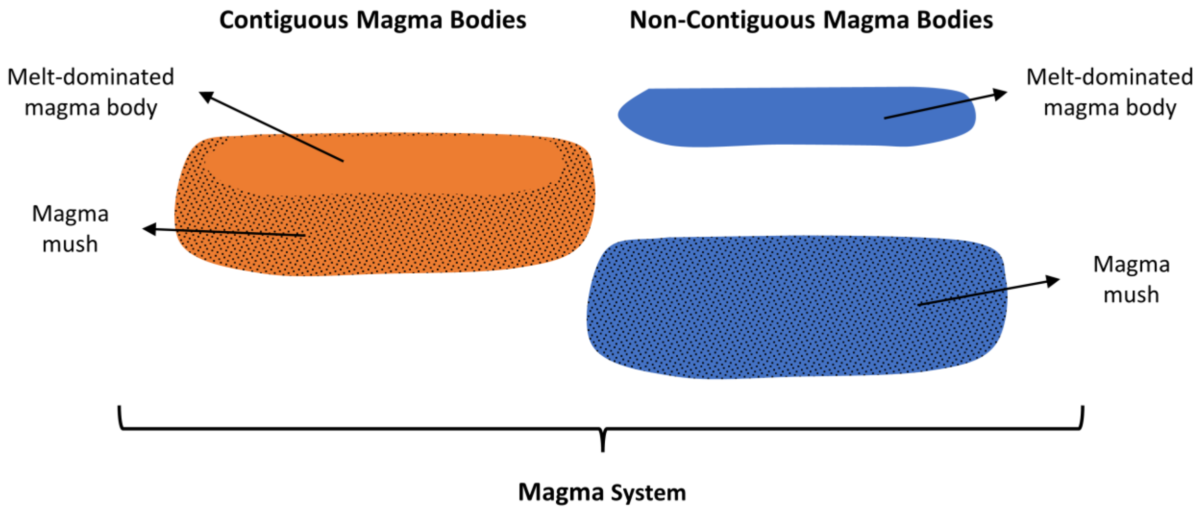

Figure 1 Schematic of a magma system and its constituents. The terms are defined in the text. In this diagram, there are two magma types, represented by the blue and orange colors.

GEOLOGIC BACKGROUND

The Taupō Volcanic Zone (TVZ) is a rifted arc (Wilson *et al.*, 1995) situated in the central North Island of Aotearoa New Zealand (Figure 2); it is one of the most active silicic volcanic regions in the world (Houghton *et al.*, 1995; Wilson *et al.*, 1995). The TVZ experienced three ignimbrite flare-ups, the most intense of which was active from ~350 to ~240 ka and included seven large ignimbrite-forming eruptions (Houghton *et al.*, 1995; Gravley *et al.*, 2007, 2016; Wilson *et al.*, 2009). This flare-up began with the largest eruptions of the young TVZ history – the Whakamaru eruptions (Wilson *et al.*, 1986; Leonard *et al.*, 2010; Downs *et al.*, 2014; Gravley *et al.*, 2016). The subsequent eruptions of this ignimbrite flare-up show a stark transition in composition and style (Wilson *et al.*, 2009; Deering *et al.*, 2010; Gravley *et al.*, 2016).

The Whakamaru magmas erupted from relatively shallow storage depths of ~50-150 MPa (Brown *et al.*, 1998; Matthews, 2011; Gualda *et al.*, 2018; Harmon *et al.*, 2024), typical of the TVZ (Bégué *et al.*, 2014b; Gualda *et al.*, 2018). The compositional change following the Whakamaru group eruptions is also marked by a change in the pressure at which the melt-dominated magma bodies feeding the caldera-forming eruptions were stored – deeper storage conditions were calculated shortly after Whakamaru eruptions, followed by a progressive shallowing through the flare-up (Gualda *et al.*, 2018; Smithies *et al.*, 2023). In the early stages of the post-Whakamaru flare-up eruptions, extraction pressures are relatively deep, with the range of extraction pressures increasing to include shallower levels over time (Gualda *et al.*, 2019; Smithies *et al.*, 2023).

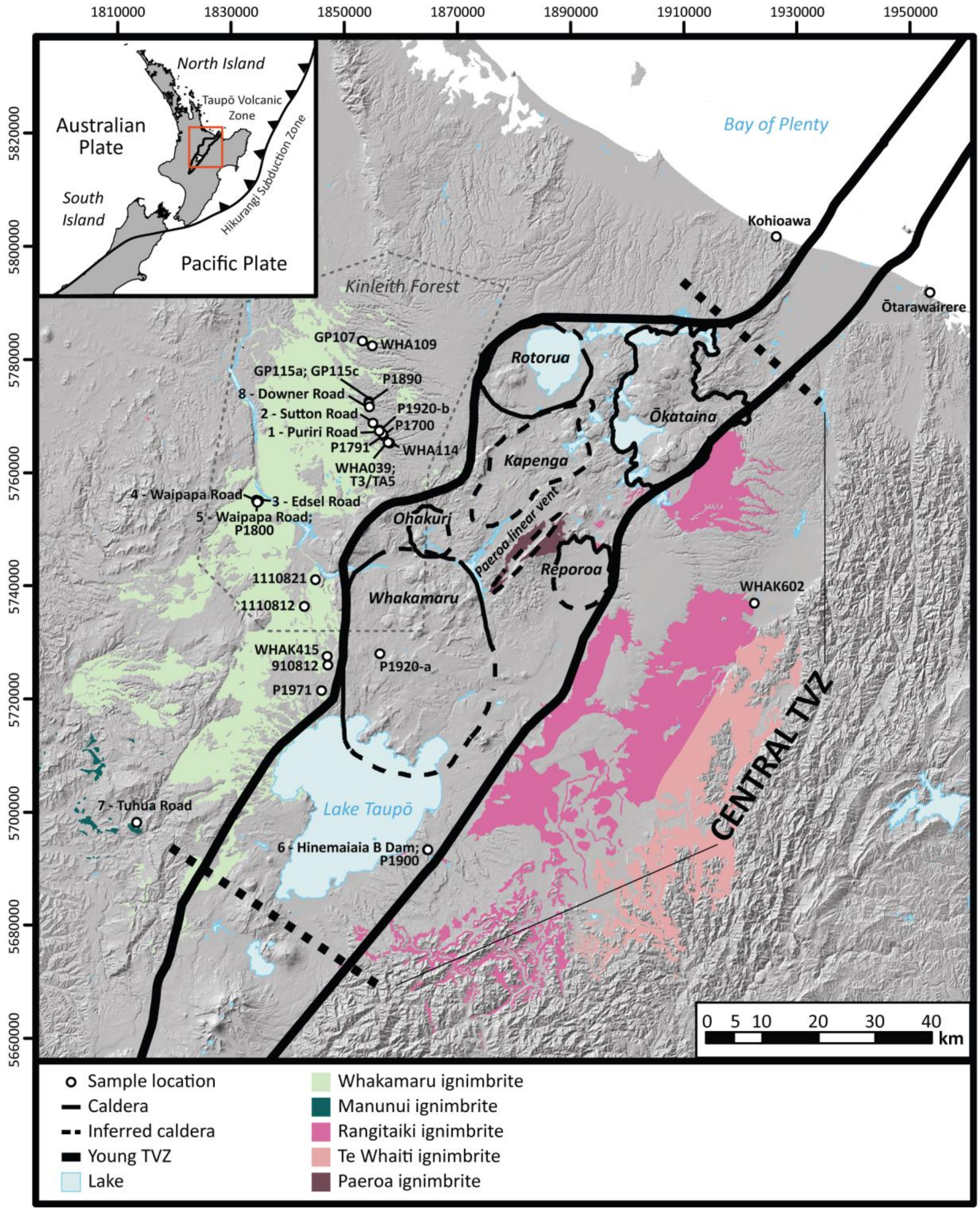

Figure 2 Map of the Taupō Volcanic Zone (TVZ), New Zealand, showing the outline of the young TVZ and major calderas of the ignimbrite flare-up (~350-240 ka). The Whakamaru group eruptions originated from the Whakamaru caldera. These eruptions

include the Whakamaru and Manunui ignimbrites distributed to the west of the caldera and the Rangitaiki and Te Whaiti ignimbrites distributed to the east of the caldera (Grindley, 1960; Wilson *et al.*, 1986; Leonard *et al.*, 2010). The younger Paeroa Subgroup erupted from the Paeroa linear vent (Downs *et al.*, 2014). Sample locations are marked, with most samples collected in the Kinleith Forest area. Samples from this study are labeled with names starting with "GP", "WHA", and "WHAK". These samples are supplemented with samples from Brown *et al.* (1998) and Matthews (2011). The two sample locations at the coast, labeled Kohioawa and Ōtarawairere, are the locations of the pyroclastic fall deposits (tephras) of Harmon *et al.*, 2024. Calderas are mapped after Leonard *et al.* (2010), outline of the young TVZ after Wilson *et al.* (1995), and the Whakamaru group ignimbrites are shown after Leonard *et al.* (2010), Brown *et al.* (1998), and Downs *et al.* (2014). Coordinate system is in meters in the New Zealand Transverse Mercator 2000 projected on the New Zealand Geodetic Datum 2000. The map inset shows the location of the TVZ within the North Island of New Zealand.

Previous work on the Whakamaru Group Ignimbrites

The Whakamaru group eruptions have long been recognized as a major volcanic event in the central TVZ (Briggs, 1976a, 1976b; Ewart & Healy, 1966; Grindley, 1960; Martin, 1965; Wilson et al., 1984, 1986, 2009). The volcanology and petrology of the Whakamaru group are complex, and the various ignimbrite deposits are notoriously difficult to place in stratigraphic order, as overlap in the field is insufficient to definitively determine their relative ages (Wilson *et al.*, 1986; Brown *et al.*, 1998). The deposits are mapped as multiple ignimbrites (Grindley, 1960; Ewart and Healy, 1966; Briggs, 1976a, 1976b; Wilson *et al.*, 1986; Brown *et al.*, 1998), but the number of eruptive phases – one (Brown *et al.*, 1998; Downs *et al.*, 2014) or multiple (Grindley, 1960; Martin, 1961; Wilson *et al.*, 1986; Houghton *et al.*, 1995) – is disputed.

There are five widespread, mappable ignimbrite units that make up the Whakamaru Group ignimbrites: the Whakamaru (*sensu stricto*), Manunui, Rangitaiki, and Te Whaiti, and the younger Paeroa Subgroup, which is interpreted to have erupted from a nearby source (Downs *et al.*, 2014) (Figure 2). We focus on the four main ignimbrites of the Whakamaru group eruptions. The three ignimbrites that have been dated (the Whakamaru, Rangitaiki, and Te Whaiti ignimbrites) have Ar-Ar age of 349 ± 4 ka (Downs *et al.*, 2014). The four ignimbrites are described in the supplementary material based on previous work (predominantly by Brown *et al.* (1998) and references therein).

Wilson *et al.* (1986) propose that the Manunui and Te Whaiti ignimbrites erupted earlier and could be correlative, while the Whakamaru and Rangitaiki ignimbrites erupted later and could be correlative. Multiple pulses have been established in both the Rangitaiki and Te Whaiti ignimbrites (Briggs, 1976b), further demonstrating the complex eruptive history of the ignimbrites.

Brown *et al.* (1998) define four compositional types of rhyolite pumice – types A, B, C, and D – with a minor amount of mingled basalt. The four types (Briggs, 1976a; Brown *et al.*, 1998) are categorized by mineralogy and whole-rock chemical composition (see supplementary material). In the Whakamaru ignimbrite, all four pumice types are found, while in the other ignimbrites, a more restricted pumice population is observed (Brown et al., 1998; Matthews, 2011).

Nomenclature

Here, the Whakamaru magma system refers to all associated melt-dominated magma bodies and magma mush bodies. We use Whakamaru group ignimbrites when referring to all the material erupted as pyroclastic flows. We specify the single Whakamaru ignimbrite when it is necessary to distinguish it from the other (i.e., Rangitaiki, Te Whaiti, Manunui) ignimbrites.

METHODS

We use matrix-glass and whole-rock compositions of individual pumice clasts to identify compositional groups, as well as to determine storage and extraction conditions. Further, we correlate our results for pumice from the ignimbrites presented here with data from co-erupted pyroclastic fall deposits (Harmon *et al.*, 2024) to constrain the timing of eruption of the various ignimbrite packages that make up the Whakamaru group ignimbrites. We sampled the largest and most pristine pumice clasts from a total of eight outcrops throughout the Whakamaru group ignimbrites, detailed in Figure 2 and supplementary material. In the field, we could not distinguish between different compositional types of pumice, so we sampled as many large pumice clasts as feasible at each outcrop. On all 39 pumice clasts, major- and trace-element glass compositions were obtained using the same methods (SEM-EDS and LA-ICPMS, respectively) as detailed in Harmon *et al.* (2024). A subset of pumice clasts (16) was analyzed via x-ray fluorescence (XRF) spectrometry to determine whole-rock compositions (see supplementary material for detailed information on the methods used). We use glass compositions from pumice clasts to calculate pre-eruptive storage pressures using rhyolite-MELTS (Gualda et al., 2012a; Bégué et al., 2014b; Gualda and Ghiorso, 2014; Pamukçu et al., 2015b; Harmon et al., 2018; Smithies et al., 2023) and pre-eruptive storage temperatures using zircon saturation geothermometry (Watson and Harrison, 1983; Boehnke *et al.*, 2013; Gualda and Ghiorso, 2013b;

Foley *et al.*, 2020; Pitcher *et al.*, 2021; Gualda *et al.*, 2022). We use glass compositions as representative of melt compositions during pre-eruptive magma storage. We use whole-rock compositions to calculate the pressure at which the melt-dominated magma was extracted from the mush (hereafter termed “extraction pressure”; see Gualda et al., 2019 and Smithies et al., 2023 and the “launching point” of Blundy, 2022) using rhyolite-MELTS. The underlying assumption is that the whole-rock compositions represent the melt extracted from the magma mush. To calculate the extraction conditions, the mineral assemblage of the magma mush must be inferred. We explore two potential magma mush mineral assemblages – one that includes quartz + feldspar (qtz-1feld) and one that includes feldspar + orthopyroxene (feld-opx). For both storage and extraction calculations, we assume magmas were fluid saturated. Gualda and Ghiorso (2014) and Ghiorso and Gualda (2015) note that qtz-1feld pressures are not a strong function of H_2O content.

RESULTS

Pumice geochemistry

Brown *et al.* (1998) define four predominant compositional pumice types – types A, B, C, and D, which are distinguished primarily based on whole-rock Rb and Sr values (see supplementary material). The pumice types are very challenging to distinguish visually in hand sample or petrographically via BSE imaging. Therefore, knowledge of whole-rock or glass compositions is necessary to determine the various magma types present. Our whole-rock data contain pumice from all four magma types, confirmed by comparing our data with those of Brown *et al.* (1998) and Matthews (2011) (Figure 3 and supplementary material). There are 6 type A pumice clasts, 7 type B pumice clasts, 2 type C pumice clasts, and 1 type D pumice clast (16 total) within our set of clasts for which we have whole-rock compositions.

In addition to the whole-rock compositions, we can distinguish types A, B, and C by their matrix glass compositions (Figure 4 and supplementary material), following the classification based on glass from pyroclastic fall deposits (i.e., tephras) correlative with the Whakamaru group ignimbrites (Harmon *et al.*, 2024). We can distinguish type A from types B and C by CaO and TiO_2 major-element glass compositions, and we can distinguish types A, B, and C (especially type B from type C) by the Ba and Sr trace-element glass compositions. Using matching whole-rock and glass pairs for several pumice clasts presented in this study, we confirm that the A, B, and C groups identified by (Harmon *et al.*, 2024) using tephra glass compositions match the original A, B, and C types identified by Brown *et al.* (1998) (Figure 5). Type D pumice clasts are distinguishable from other pumice types in whole-rock composition but are not readily distinguishable by the glass compositions (as glass compositions are very similar to those of type A). Since we have whole-rock data for only one type D pumice clast, we cannot definitively distinguish type D pumice clasts from type A pumice clasts for which we do not also have whole-rock compositions. However, type D is considered much less abundant than type A in the Whakamaru group ignimbrites (Brown *et al.*, 1998).

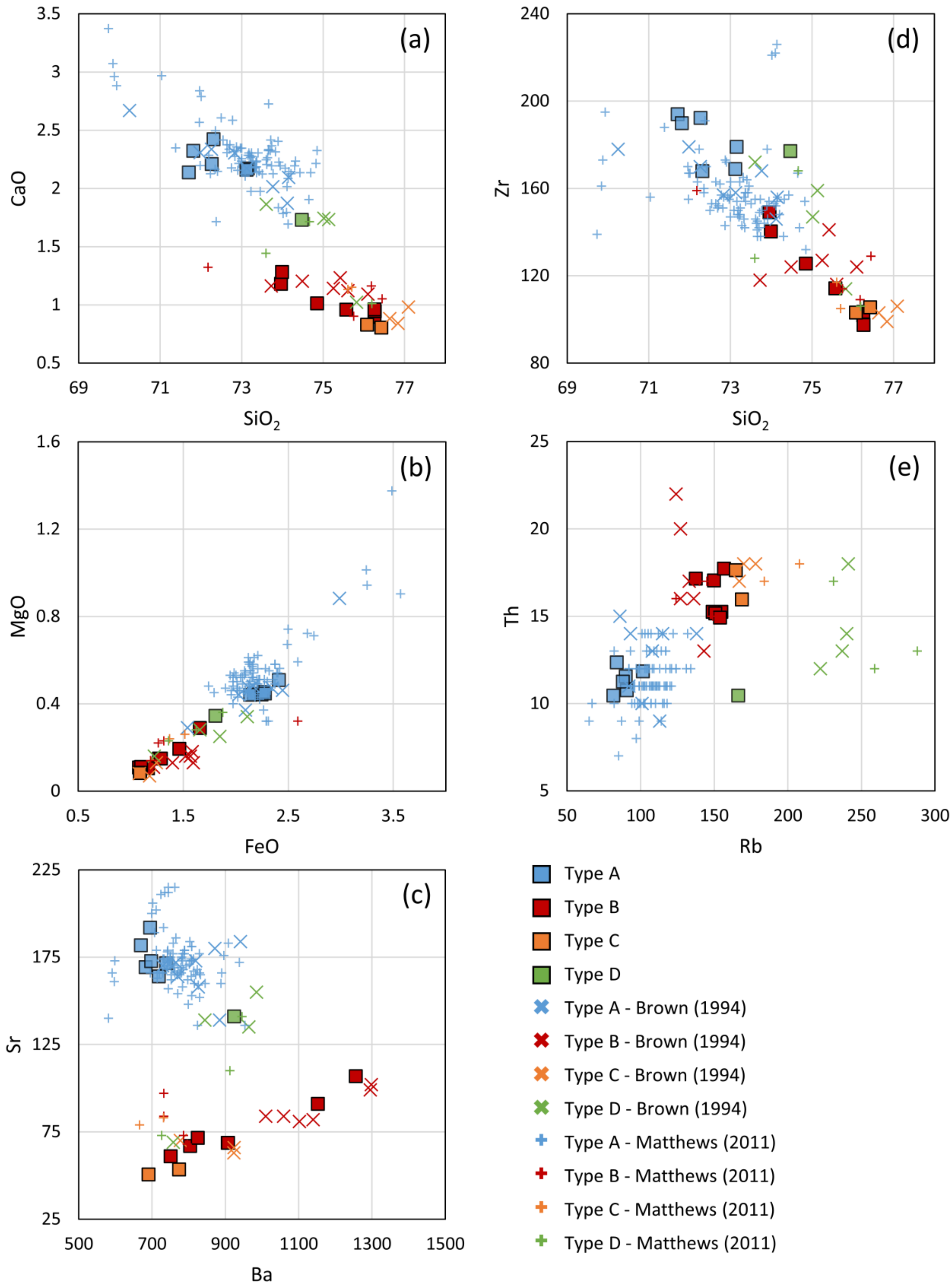

(a)
CaO
SiO2
(d)
Zr
SiO2
(b)
MgO
FeO
(e)
Th
Rb
(c)
Sr
Ba
Type A
Type B
Type C
Type D
Type A - Brown (1994)
Type B - Brown (1994)
Type C - Brown (1994)
Type D - Brown (1994)
Type A - Matthews (2011)
Type B - Matthews (2011)
Type C - Matthews (2011)
Type D - Matthews (2011)

247

Figure 3 Whole-rock compositions of pumice clasts from the Whakamaru group ignimbrites. Major elements (SiO_2, CaO, FeO, MgO) are reported as weight percent (wt. %) of the oxide normalized anhydrous; trace elements (Zr, Th, Rb, Sr, Ba) are reported in parts per million (ppm). Data presented here are represented by filled-in squares. Data from Brown (1994) are represented by x's. Data from Matthews(2011) are represented by +'s. The four compositional groups (types A, B, C, D) are established from Brown *et al.* (1998) and are represented by colors, where type A is blue, type B is red, type C is orange, and type D is green. Type B and type C contain sanidine; all types contain quartz and plagioclase (Brown *et al.*, 1998).

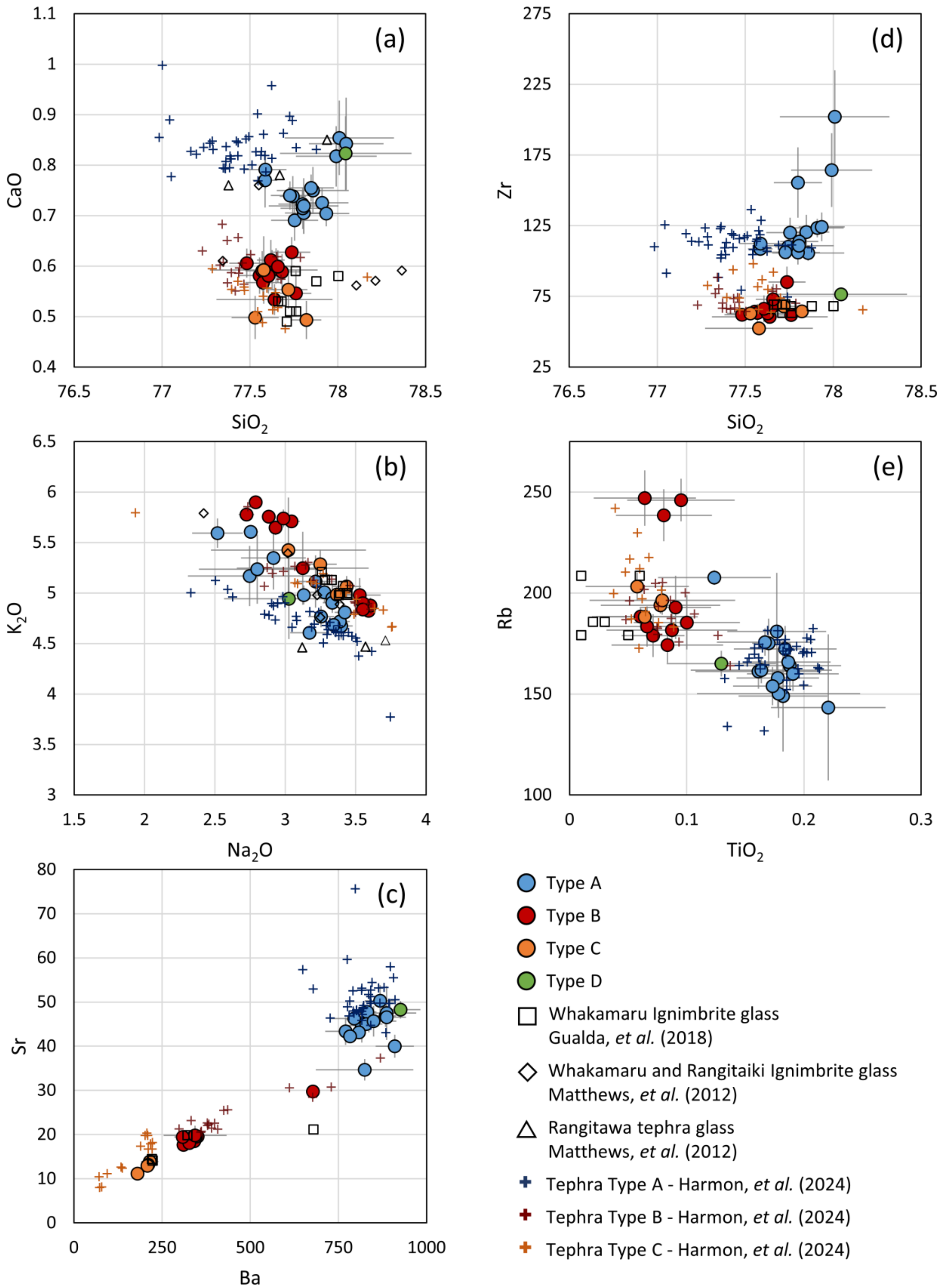
(a)
CaO
SiO_2
(d)
Zr
SiO_2
(b)
K_2O
Na_2O
(e)
Rb
TiO_2
(c)
Sr
Ba
Type A
Type B
Type C
Type D
Whakamaru Ignimbrite glass Gualda, *et al.* (2018)
Whakamaru and Rangitaiki Ignimbrite glass Matthews, *et al.* (2012)
Rangitawa tephra glass Matthews, *et al.* (2012)
Tephra Type A - Harmon, *et al.* (2024)
Tephra Type B - Harmon, *et al.* (2024)
Tephra Type C - Harmon, *et al.* (2024)

257

Figure 4 Major- and trace-element glass compositions from pumice clasts of the Whakamaru group ignimbrites. Major elements (SiO_2, CaO, K_2O Na_2O, TiO_2) are reported as wt.% of the oxide normalized anhydrous; trace elements (Zr, Rb, Sr, Ba) are reported in ppm. The four types (A, B, C, D) are established from whole-rock composition data from pumice clasts that have matching glass and whole-rock data. Data from tephra deposits correlated to the Whakamaru eruptions from Harmon *et al.* (2024) are represented by +'s. Whakamaru ignimbrite glass data from Gualda *et al.* (2018) are represented by small squares. From Matthews *et al.* (2012), ignimbrite data are represented by small triangles and Rangitawa tephra data are represented by small diamonds.

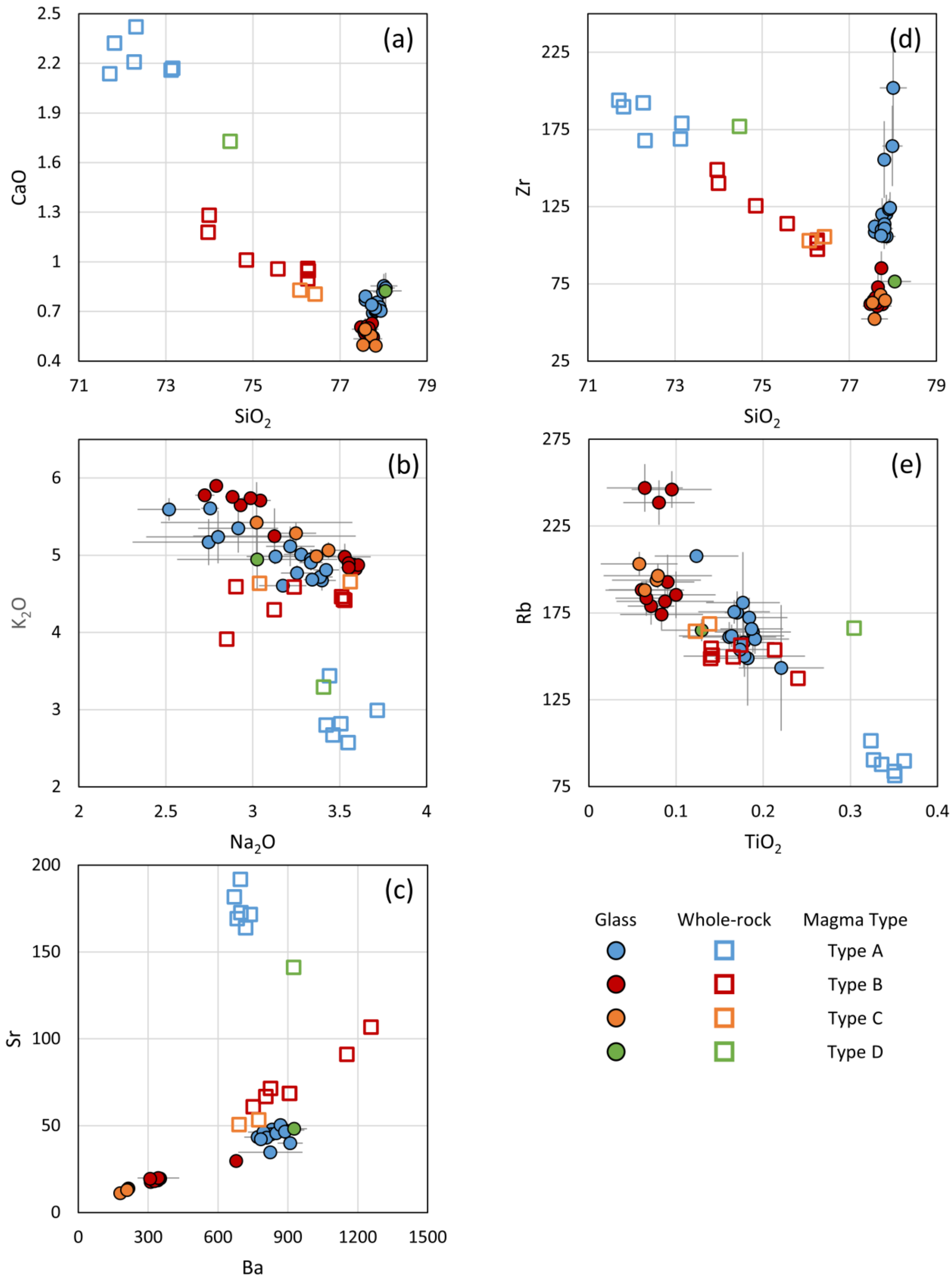
(a)
CaO
SiO_2
(d)
Zr
SiO_2
(b)
K_2O
Na_2O
(e)
Rb
TiO_2
(c)
Sr
Ba
Glass
Whole-rock
Magma Type
Type A
Type B
Type C
Type D

Figure 5 Glass and whole-rock compositional data from Whakamaru group ignimbrite pumice clasts. Major elements (SiO_2, CaO, K_2O Na_2O, TiO_2) are reported as wt.% of the oxide; trace elements (Zr, Rb, Sr, Ba) are reported in ppm. Whole-rock data are represented by squares; glass data are represented by filled circles. Data are subdivided into types A, B, C, and D based primarily on whole-rock compositions. The pumice clasts for which we only have compositional data for glass are subdivided based on their chemical similarity to pumice clasts with both whole-rock and glass compositions.

Distribution of pumice types

The Whakamaru ignimbrite (*sensu stricto*) has pumice from all four compositional types (types A, B, C, D). From the pumice analyzed in previous studies, the Manunui ignimbrite has 1 type A, 1 type C, and 2 type D samples (Brown *et al.*, 1998; Matthews, 2011), and the Rangitaiki ignimbrite contains exclusively type A pumice (Brown, 1994; Brown *et al.*, 1998; Matthews, 2011) (Figure 6). We did not analyze pumice clasts from Te Whaiti pumice due to the welded nature of the deposits, and there is limited information available in the literature (Brown, 1994; Brown *et al.*, 1998; Matthews, 2011).

The various outcrops of the Whakamaru ignimbrite show possible variation in the proportion of different pumice types (Figure 6). In the northwest portion of the deposits (i.e., Kinleith forest, outlined in Figures 2 and 6), there is a concentration of outcrops that have type C pumice in addition to types A and B pumice clasts, with many outcrops exhibiting more than one type of pumice. The majority of the western and southern Whakamaru deposits are dominated by type A and type B pumice, with smaller abundance of type D pumice (Figure 6 and supplementary material).

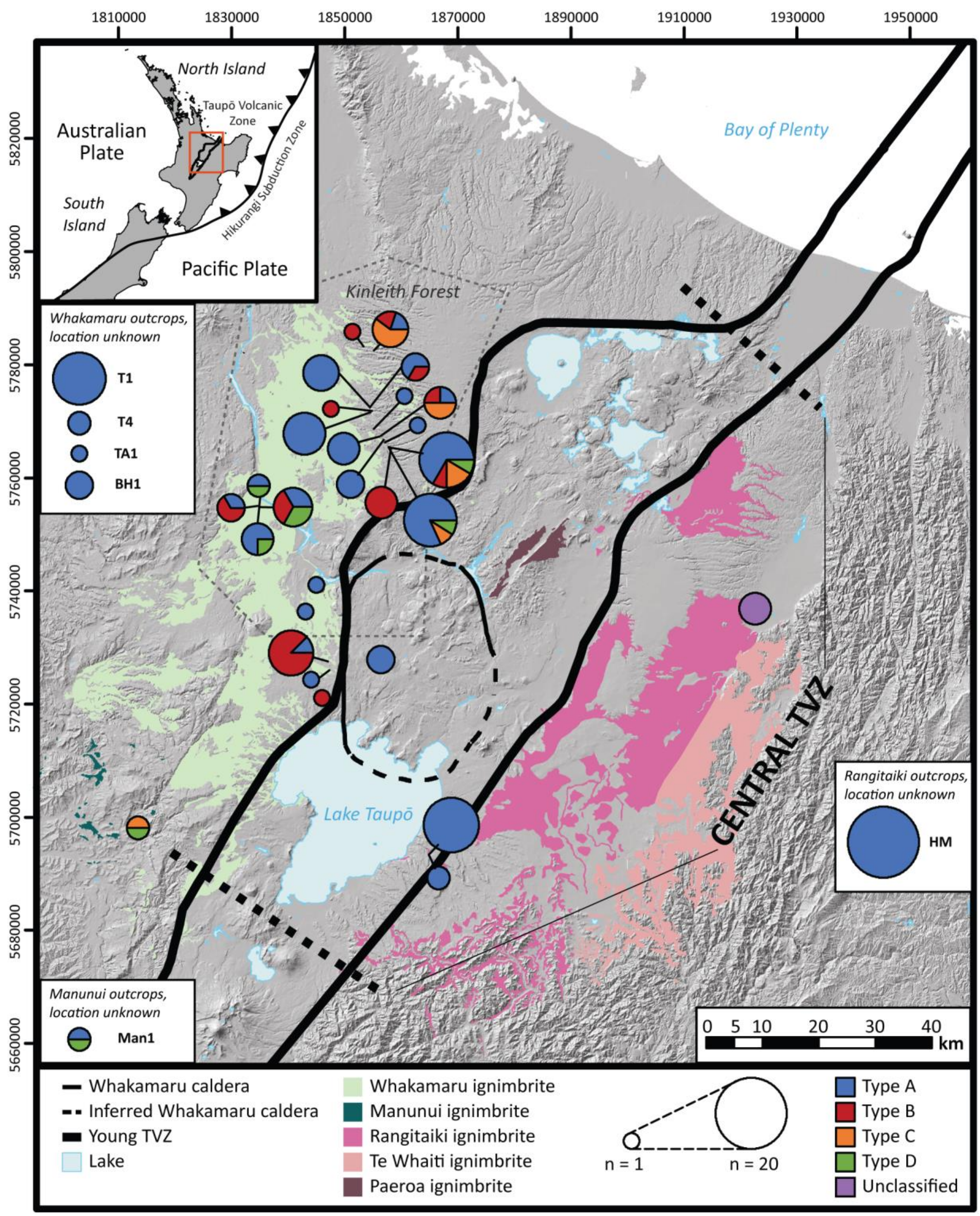

Figure 6 The distribution of pumice types at the different sampling locations. The colors of the pie-charts represent the different pumice types (types A, B, C, D), and the size of the pie chart represents how many pumice clasts are analyzed at each location. The

Kinleith forest area has the highest sampling density, to the north of the caldera within the Whakamaru ignimbrite. Five sample locations from Matthews (2011) are unknown, although the ignimbrite from which they were collected is known. Therefore, the samples from those locations are shown in white boxes near the ignimbrite from which they were collected.

Geobarometry

Storage assemblages and pressures

Overall, storage pressures calculated from glass compositions are shallow, ranging from 45-140 MPa (1.7-5.4 km depth, assuming a crustal density of $2.7*10^3$ kg/m^3; Stagpoole et al., 2021) (Figure 7 and supplementary material). We calculate average storage pressures of 92 ± 18 MPa (1-sigma) (3.5 ± 0.7 km) for type A, 118 ± 23 MPa (4.5 ± 0.9 km) for type B, 94 ± 19 MPa (3.6 ± 0.7 km) for type C, and 75 MPa (2.8 km) for type D.

Previous studies (Ewart, 1965; Martin, 1965; Briggs, 1976a; Brown *et al.*, 1998) demonstrate that pumice types A and D do not have sanidine, while types B and C do have sanidine. Therefore, types A and D should not produce qtz-2feld storage pressures, and the qtz-1feld assemblage is expected for the storage pressures. This pattern is consistent with what is observed in the correlative fall-derived tephras studied by Harmon *et al.* (2024).

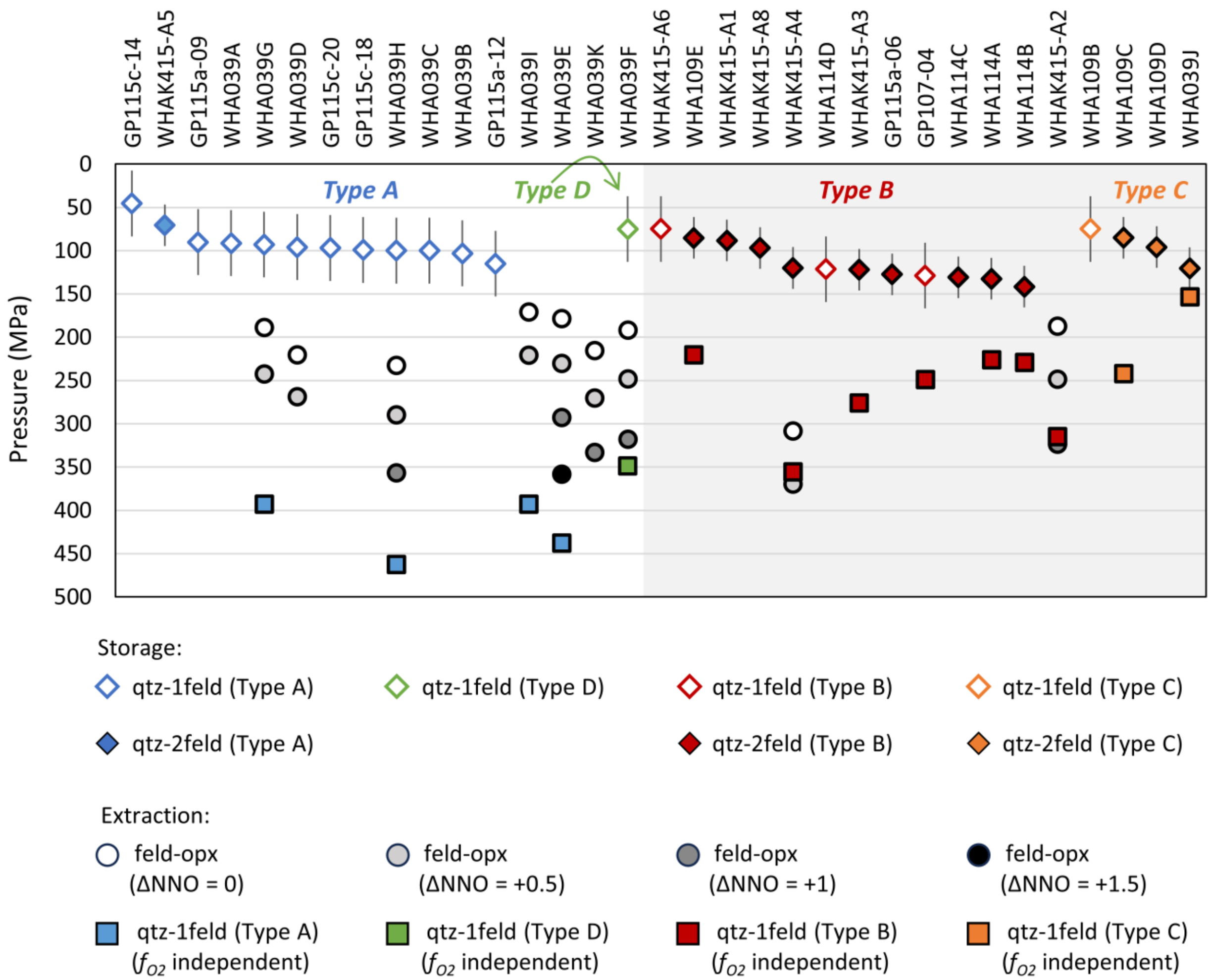

Figure 7 Rank-order diagram of magma storage and extraction pressures from rhyolite-MELTS calculations. Storage pressures are represented by diamonds with qtz-1feld storage assemblage represented by open diamonds qtz-2feld storage assemblage represented by filled diamonds. The extraction pressures represented by circles (feld-opx extraction assemblage) and squares (qtz-1feld extraction assemblage) show from what depth the melt was extracted from the magma mush bodies. The feld-opx extraction pressures are dependent on f_{O2}. The circles represent the feld-opx extraction pressures at increasing f_{O2} (ΔNNO 0 = white, ΔNNO +0.5 = light gray, ΔNNO +1 = dark gray, and ΔNNO + 1.5 = black). The colored squares represent the qtz-1feld extraction pressures,

which are not dependent on f_{O2}. The qtz-1feld extraction pressures represent the deepest possible extraction pressures in this case. Magma types A and D have an extraction assemblage of feld-opx at lower f_{O2} and feld-opx±qtz at higher f_{O2} (ΔNNO +1.5). Magma types B and C have an extraction assemblage of qtz-1feld.

Extraction assemblages and pressures

We consider two possible extraction assemblages – quartz + feldspar (qtz-1feld) or feldspar + orthopyroxene (feld-opx) – both of which are considered potential assemblages for the TVZ mush bodies that sourced the melt-dominated magma bodies (Gualda *et al.*, 2019; Smithies *et al.*, 2023). Extraction pressures and assemblages are reported in Figure 7 and supplementary material. Calculated extraction pressures depend on the extraction assemblage considered and oxygen fugacity (f_{O2}).

For almost all pumice clasts of types B and C, qtz-1feld extraction pressures are lower than corresponding feld-opx extraction pressures (Figures 7 and 8). In these cases, we only consider qtz-1feld extraction pressures (see discussion for details), which yield extraction pressures in the range of 155-355 MPa (5.8-13.4 km), with most pressures in the 220-310 MPa (8.3-11.7 km) range.

For almost all pumice clasts of types A and D, feld-opx extraction pressures can be lower than qtz-1feld extraction pressures. In these cases, we consider feld-opx extraction pressures as a function of f_{O2}.The feld-opx extraction pressures increase with increasing f_{O2} due to the geometry of the orthopyroxene saturation curve relative to the feldspar and quartz saturation curves (Figure 8). We calculate the following range of extraction pressures for types A and D, which produce extraction pressures with a feld-opx assemblage: 170-235 MPa (6.5-8.8 km) for ΔNNO = 0, 220-290 MPa (8.3-10.9 km) for ΔNNO = +0.5, 290-355 MPa (11.0-13.5 km) for ΔNNO = +1, and

360 MPa (13.5 km) for ΔNNO = +1.5. One composition produces a feldspar + orthopyroxene + quartz (feld-opx-qtz) pressure (316 MPa for ΔNNO +1, 347 MPa for ΔNNO +1.5). The qtz-1feld pressures for types A and D are in the range 350-465 MPa and are the deepest extraction pressures calculated.

349

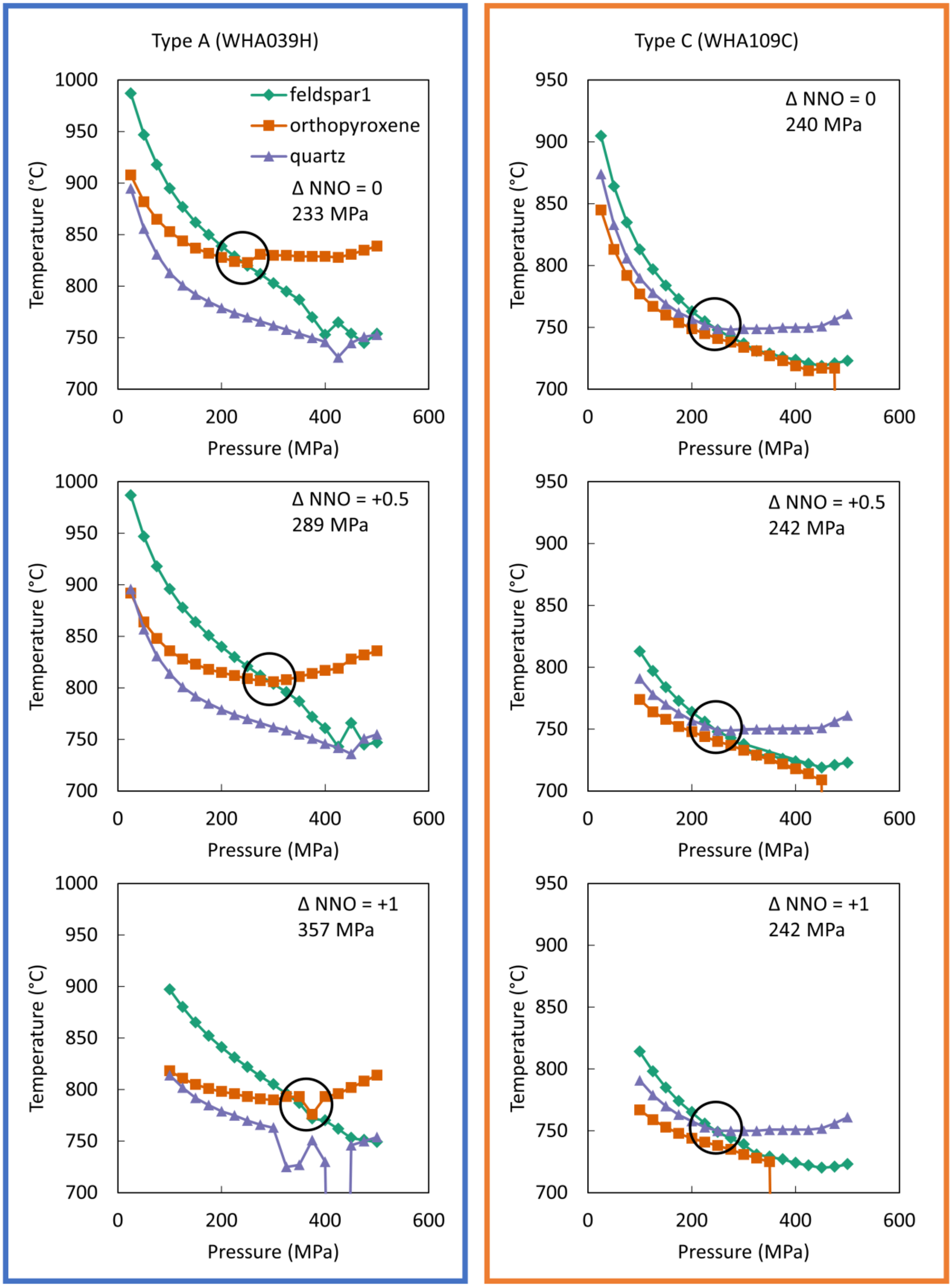
Type A (WHA039H)
Type C (WHA109C)
feldspar1
orthopyroxene
quartz
Δ NNO = 0
233 MPa
Δ NNO = 0
240 MPa
Δ NNO = +0.5
289 MPa
Δ NNO = +0.5
242 MPa
Δ NNO = +1
357 MPa
Δ NNO = +1
242 MPa
Temperature (°C)
Pressure (MPa)

Figure 8 Representative rhyolite-MELTS extraction pressure calculations cast in temperature versus pressure space. The panels on the left (blue box) illustrate representative type A extraction calculations; the panels on the right (orange box) illustrate representative type C extraction calculations. In each diagram, the lines represent saturation surfaces of specific minerals (feldspar, orthopyroxene, and quartz). The intersection (between the feldspar and orthopyroxene curves for type A and between feldspar and quartz for Type C; indicated by the black circle) indicates the pressure conditions of extraction for a given composition and f_{O2}. For each composition, we show three different calculations, at different f_{O2} values. For each calculation, f_{O2} is constrained; in the top row, f_{O2} is equal to NNO, and then increases to ΔNNO +0.5 in the middle row and to ΔNNO +1 in the bottom row. The left column illustrates that type A extraction pressures are dependent on f_{O2}, as the orthopyroxene saturation curve intersects the plagioclase saturation curve but not the quartz saturation curve, and the orthopyroxene curve is sensitive to f_{O2}. In the type C panel, orthopyroxene always saturates at a lower temperature than quartz and feldspar. Therefore, orthopyroxene is not considered as part of the extraction assemblage in the type C cases. See Gualda *et al.* (2019) for a detailed description of the method.

Zircon-saturation temperatures

Zircon was likely saturated in all magma types (Brown, 1994), which is supported by our whole-rock and glass pairs, which show lower Zr concentrations in glass when compared to whole-rock, indicating that some Zr is fractionated into zircon (Figures 5 and 9) (Foley *et al.*, 2020). All individual calculations are reported in the supplementary material. Generally, we see that types A samples are relatively hotter by ~40-60 °C, while types B, C, and D are relatively cooler. Using the average glass compositions, we calculate zircon saturation temperatures of 771 ± 17 °C (1-sigma) for type A, 720 ± 9 °C for type B, 715 ± 8 °C for type C, and 733 °C for the type D sample using the Watson and Harrison (1983) calibration. Using the Boehnke *et al.* (2013) calibration, the average zircon saturation temperatures are 725 ± 20 °C (1-sigma) for type A, 665 ± 10 °C for type B, 660 ± 9 °C for type C, and 682 °C for type D.

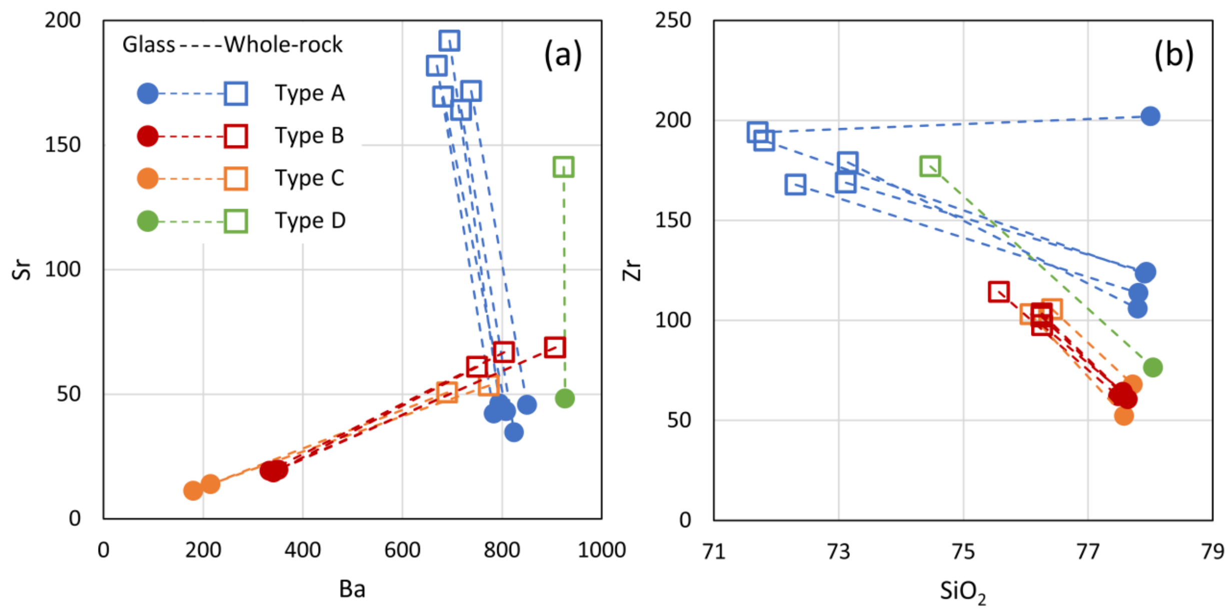

Figure 9 Compositional data for individual pumice clasts that have both whole-rock and glass compositions in a) Sr vs Ba and b) Zr vs SiO_2 space. SiO_2 is reported as wt.% of the oxide; trace elements (Sr, Ba, Zr) are reported in ppm. The whole-rock compositions are represented by open squares, and the glass compositions are represented by filled circles; dashed lines connect corresponding whole-rock and glass compositions. The different pumice compositional types (A, B, C, D) are represented by different colors. These diagrams suggest that all magmas were saturated in plagioclase, quartz, and zircon, as evidenced by the lower concentrations of Sr, Zr, and SiO_2 in glass relative to whole rock.

However, only types B and C were also saturated in sanidine, as evidenced by the lower concentration of Ba in these glasses relative to whole rock.

DISCUSSION

Pre-eruptive storage conditions of the melt-dominated magma bodies

Four distinct types of magma sourced the Whakamaru eruptions (Brown *et al.*, 1998). Our samples can first be categorized into two overarching geochemical groups based on whole-rock and glass compositions, as well as mineralogy. Samples of pumice types A and D form the first group. They have higher Sr and CaO in whole-rock compositions (Figures 2 and 9) and higher Sr, Ba, and Zr in glass compositions in comparison to types B and C (Figures 3 and 9). Pumice clasts of types B and C form a second group, having lower Sr and Zr in whole-rock compositions (Figures 2 and 9), generally more fractionated glass compositions with lower Ba and Sr and slightly higher Rb (Figure 4). These characteristics are consistent with the presence of sanidine in types B and C, and the absence of sanidine in types A and D (Brown *et al.*, 1998; Harmon *et al.*, 2024).

The paired whole-rock and glass compositions from the individual pumice clasts provide evidence for the saturation (or undersaturation) of various mineral phases in the different magma types. The presence of zircon is ubiquitous in all four magma types, as evidenced by the higher concentration of Zr in the whole rock in comparison to the glass of the same pumice clasts (Figure 9). Zr is a major constituent of the mineral zircon, so a lower concentration in the glass implies that a portion of the Zr is contained within zircon crystals in the pumice clast. A similar argument can be made for the presence of the feldspars – plagioclase and sanidine. All four magma types have a lower concentration of Sr in the glass when compared to the whole-rock compositions, indicating that all four magma types were saturated in plagioclase. Due to the preferential uptake of Ba in sanidine, lower Ba contents in the glass relative to whole-rock demonstrate sanidine saturation in types B and C, while types A and D show higher Ba in glass than whole-rock, consistent with absence of sanidine (see Figure 9). This matches the well-established mineralogy (from Brown *et al.*, 1998 and references therein) and confirms the inferences from Harmon *et al.* (2024) based on rhyolite-MELTS storage pressure calculations that type A does not contain sanidine while types B and C are sanidine-bearing. The presence of sanidine is unusual within the TVZ, with the Whakamaru group ignimbrites being one of the few units to contain sanidine-bearing pumice.

Results for rhyolite-MELTS storage pressures presented here support the distribution of sanidine in the different pumice types. Most storage pressures for types A and D are not sanidine-bearing (producing qtz-1feld pressures, Figures 7 and 10), while most storage pressures for types B and C are sanidine-bearing (producing qtz-2feld pressures, Figures 7 and 10). This suggests that – at least in the case of the Whakamaru group magmas – rhyolite-MELTS can be effectively used to infer the felsic mineralogy in equilibrium with each magma type, which is particularly useful when direct observation is not possible (Harmon *et al.*, 2024). While the glass compositions are consistent with the observed mineralogy and rhyolite-MELTS calculations, we do not have quantitative information on the amounts and volumes of minerals, so we can only say that the glass compositions are qualitatively consistent with the matching whole-rock compositions (Figure 9). Zircon-saturation geothermometry helps to further parse these groups (supplementary material). The results suggest that type A was stored at a hotter temperature (~40-60 °C hotter) than types B, C, and D. Together, the geothermometry and geobarometry results suggest at least 3 distinct melt-dominated magma bodies (A, B+C, D). Despite overlapping storage assemblages and pressures, the distinct trace-element glass compositions of types B and C (Figures 4 and 9) suggest they were likely two different melt-dominated magma bodies, indicating that the four magma types represent at least four magma bodies. Since there is little overlap in either whole-rock or glass compositions among the different magma types, the melt-dominated magma bodies likely did not mix prior to eruption (see also Harmon *et al.*, 2024).

Considering the rhyolite-MELTS geobarometry results in more detail also provides some insights into the arrangement of these magma bodies in the crust. The rhyolite-MELTS storage pressures are all similarly shallow (Figures 7 and 10), indicating that each magma type occupied a narrow range of storage depths in the upper crust. This is consistent with the predominantly shallow storage pressures of caldera-forming rhyolite magmas in the central TVZ (Bégué *et al.*, 2014a). Interestingly, there is no difference in the pressure distribution between the three main magma types (A, B, and C; Figure 10), consistent with the findings of Harmon *et al.* (2024) that the Whakamaru group eruptions were fed by laterally juxtaposed melt-dominated magma bodies – and in contrast with the vertically stratified single magma chamber model advocated by Brown *et al.* (1998). This adds to the growing evidence that very large to supereruptions (VEI >6) can be fed by a patchwork of melt-dominated magma bodies (Cooper *et al.*, 2012, 2017; Gualda and Ghiorso, 2013b; Bégué *et al.*, 2014a; Wotzlaw *et al.*, 2014; Swallow *et al.*, 2018; Pearce *et al.*, 2020; Gualda *et al.*, 2022).

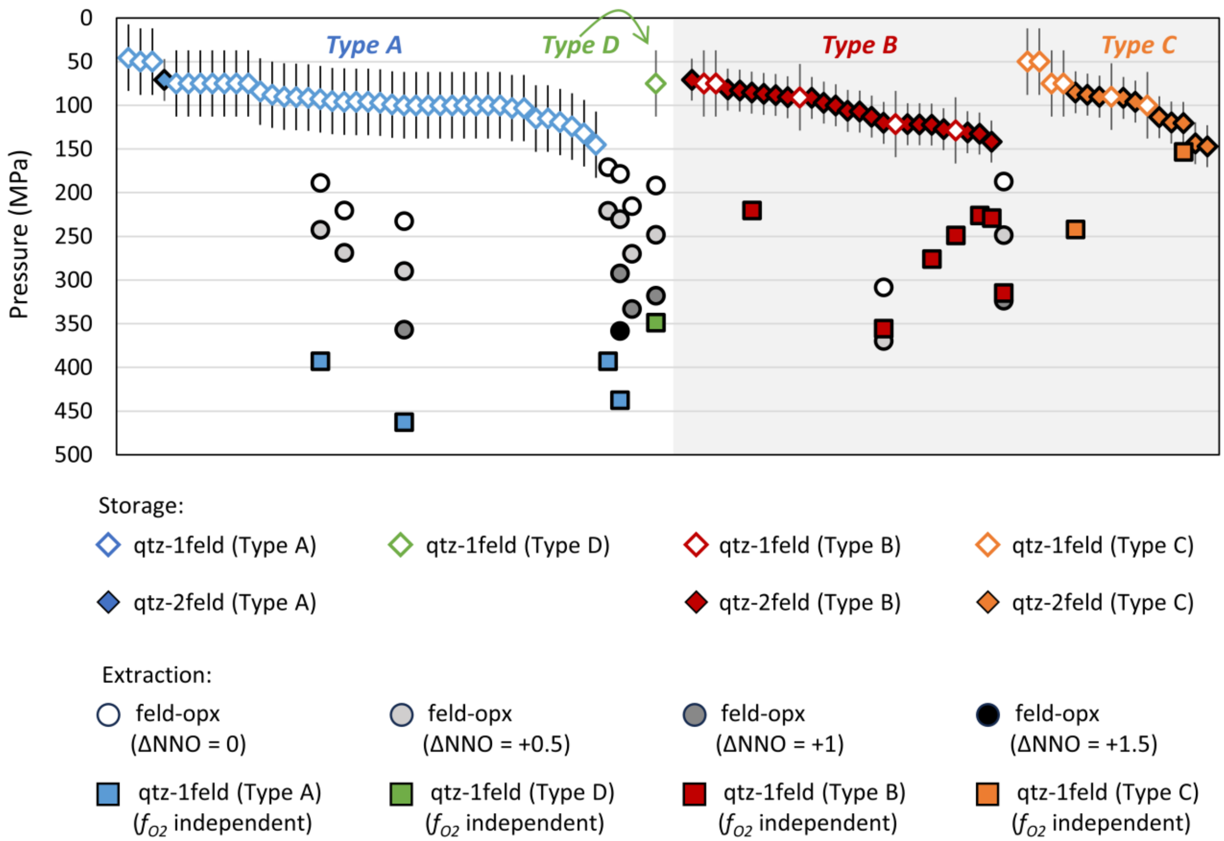

Figure 10 Magma storage and extraction pressures from rhyolite-MELTS calculations, represented by the rank-order of the storage pressures from this work and from Harmon *et al.* (2024). See Figure 7 for an explanation of the symbology and modeling details. The combination of the data from the tephra and from the ignimbrites shows consistent storage pressures for the Whakamaru group eruptions.

Extraction conditions and the depths of magma mush bodies

Extraction pressures provide insight into the organization of magma mush bodies in the crust as a function of depth, as well as – when combined with storage pressures – their positions relative to the melt-dominated magma bodies extracted from them (Figures 10 and 11) (Gualda *et al.*, 2019; Smithies *et al.*, 2023). Previous work in the TVZ shows that both contiguous and non-contiguous storage has occurred in the region (Gualda *et al.*, 2019; Smithies *et al.*, 2023).

We find that extraction pressures for types B and C are independent of f_{O2}, given that qtz-1feld pressures are lower than feld-opx pressures for plausible f_{O2} values (ΔNNO from 0 to +1.5). Type B magma extraction occurred at depths in the range of 220-360 MPa (~8-13 km), and type C extraction occurred at depths in the range of 150-240 MPa (~5.5-9.0 km). This suggests predominantly non-contiguous extraction for types B and C, with some type C magma potentially exhibiting contiguous extraction and storage (Figures 10 and 11).

Types A and D magmas are distinct from types B and C in their extraction characteristics. For type A and D compositions, extraction pressures for a plagioclase + orthopyroxene (feld-opx) assemblage are typically lower (indicating shallower extraction) than for a qtz-1feld assemblage, suggesting equilibration with an assemblage consisting of plagioclase and orthopyroxene. Due to the sensitivity of orthopyroxene stability on f_{O2} conditions, extraction pressures increase with increasing f_{O2} (Figure 8). For the range of f_{O2} that we tested for (ΔNNO equal to 0 to +1.5), resulting extraction pressures vary from 170 MPa to 460 MPa for types A and D magmas. We are left with two competing hypotheses:

1. If f_{O2} is lower (ΔNNO < 1), all magma types are extracted from a shallower depth (~150-360 MPa) with two different assemblages: types A and D extracted from a mush with a feld-opx assemblage; types B and C extracted from a mush with a qtz-1feld assemblage
2. If f_{O2} is higher (ΔNNO > 1), the magmas are extracted from different depths with different assemblages: types A and D extracted from a mush up to ~290-460 MPa with feld-opx±qtz and types B and C still extracted from ~150-360 MPa from a mush with a qtz-1feld assemblage

A lower f_{O2} (ΔNNO < 1) is consistent with the estimates by Matthews (2011). This would imply that the different magma types are extracted from similar crustal levels with different assemblages, which could signal that there is a tectonic or structural control of where in the crust the mush bodies develop. If the f_{O2} is higher (ΔNNO > 1), which agrees with the estimates by Brown *et al.* (1998) and Deering *et al.* (2010), then the source of type A and D magmas likely included feldspar + orthopyroxene ± quartz at deeper pressures, implying that the base of the TVZ crust is saturated in quartz for this system. In either scenario, the extraction of types A and D occurs over a narrow range.

Both SiO_2 concentrations in the whole-rock compositions and zircon saturation temperatures can help constrain which extraction scenario is more likely. The relatively wide range of SiO_2 whole-rock compositions for type A and type D indicate that quartz is likely not present (undersaturated) at the source, in contrast with the case of the Taupō Ignimbrite (see Pamukçu *et al.*, 2021), in which the SiO_2 concentration in the whole-rock compositions are tightly constrained within ~1 wt% SiO_2, indicating that quartz is present (saturated) at the source. If quartz is not present at the source, then the f_{O2} values of Matthews (2011) and the lower end of the f_{O2} values from Deering *et al.* (2010) are more likely. This provides evidence for all magma types being extracted from a relatively similar, shallower level (Figure 11). It is difficult to ascertain if the magma mush bodies were saturated in zircon or not; nonetheless, the higher Zr contents of whole-rock type A pumice suggests that extraction temperatures could have been higher for type A when compared to types B and C magmas.

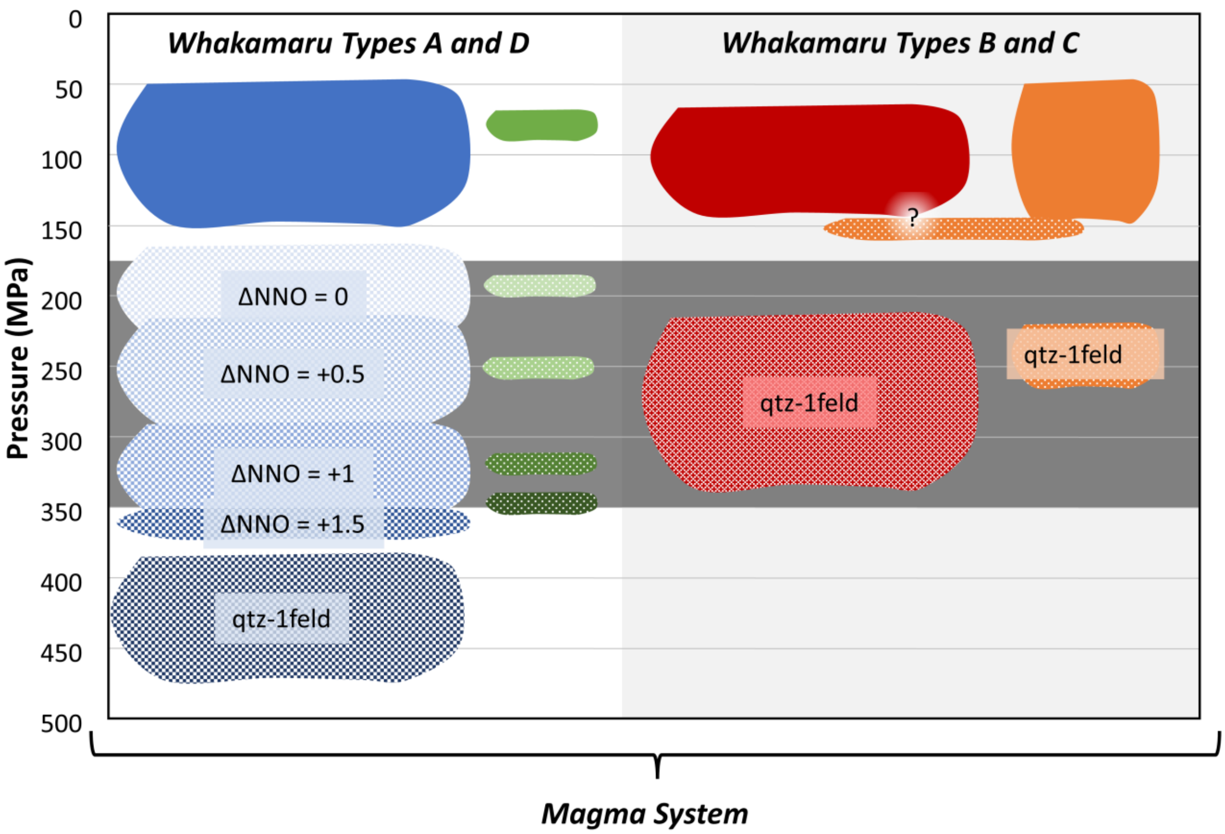

Figure 11 Schematic of the Whakamaru magma system. Melt-dominated magma bodies were stored at shallow storage pressures (~50-150 MPa) and are represented by solid colors. The four magma types represent at least four different magma bodies. The textured magma bodies represent the deeper magma mush bodies, from which the melt-dominated magmas were extracted. From the extraction assemblages and compositions of the pumice clasts, types A and D were part of one magma subsystem with an extraction assemblage of feld-opx±qtz, and types B and C were part of a different subsystem with an extraction assemblage of qtz-1feld. The extraction pressures for types A and D are dependent on f_{O2}, with the shallower magma mush body representative of a lower f_{O2}, and the deeper extraction depth representing a higher f_{O2}. Independent f_{O2} estimates indicate that an f_{O2} of ΔNNO = ~+0.5 to +1 is more likely (Matthews, 2011). The most likely

extraction pressure range is highlighted in dark gray (~175-350 MPa). All four magma types experienced non-contiguous extraction and storage. There is a possibility that a portion of type C magma also experienced contiguous extraction and storage, represented by the highlighted question mark and discussed in the text.

The timing of the Whakamaru eruptions

Understanding the temporal relations of the Whakamaru group ignimbrites is difficult given the lack of distinctive field relationships between the different ignimbrites (Briggs, 1976a, 1976b; Brown et al., 1998; Leonard et al., 2010; Wilson et al., 1986). However, we can take advantage of pyroclastic fall deposits from the Kohioawa and Ōtarawairere locations in the Bay of Plenty (Figure 2) that have been correlated with the Whakamaru group ignimbrites (Manning, 1995, 1996; Harmon *et al.*, 2024) to constrain the relative timing of the ignimbrites by matching magma types, mineralogy, and glass compositions from the tephra with the characteristics of the ignimbrites.

Evidence from the tephra shows that there are three main phases of the Whakamaru eruptions (Harmon *et al.*, 2024). To summarize, type A continuously erupts throughout the Whakamaru eruptions, while type B appears in the second and third tephra units. Type C is a late-erupted magma type that only erupts in the third unit of the tephras – it is the dominant magma type at that stage. Since we cannot distinguish type A from type D using only glass compositions, we cannot determine where in the stratigraphy type D magma erupts.

Since evidence from the tephra deposits requires that no sanidine-bearing magma be erupted during the first stages of the eruption (correlative with the first tephra unit; see Harmon *et al.*, 2024), only types A and D can erupt in the first phase. Since the Rangitaiki ignimbrite exhibits only type A (Brown, 1994; Brown *et al.*, 1998; Matthews, 2011), it is most likely correlative with the first tephra unit, leading us to conclude that it erupted early in the sequence. This implies that the Rangitaiki ± Te Whaiti ignimbrites preserved in the east likely erupted first due to the lack of sanidine and confirms the interpretation by Wilson *et al.* (1986) that the Te Whaiti was part of the earliest eruptions. However, more evidence from the Te Whaiti deposits is required to definitively interpret the deposits as the first ignimbrites of the sequence. There are also several outcrops from the Whakamaru ignimbrite (including the samples from unknown Whakamaru ignimbrite locations from Matthews, 2011) that contain exclusively type A pumice clasts, which is consistent with the base of the Whakamaru drill core lacking sanidine (Grindley, 1960; Ewart and Healy, 1966; Brown *et al.*, 1998). There are likely earlier eruptive pulses to the west as well as the east, although we note that there are relatively few (<5) pumice clasts from each of these type A-only outcrops to the west from this study, which may not be representative of the pumice types present at these locations. In these locations, it is possible that these pulses of Whakamaru ignimbrite are correlative with the earliest eruptive phase.

The middle tephra package has clasts of types A and B compositions but no type C compositions (Harmon *et al.*, 2024). The western Whakamaru ignimbrite deposits exhibit types A, B, and D, with no type C pumice clasts (Figure 6), indicating that these ignimbrite deposits correlate to the middle (and main pulse of) Whakamaru eruptions.

Clasts with type C magmas are only found in the upper tephra package (Harmon *et al.*, 2024). Both the Manunui ignimbrite in the southwest and the Whakamaru ignimbrite in the northernmost samples on the west side of the TVZ (the Kinleith forest area) contain type C pumice. Type C pumice is abundant in several Kinleith sampling locations, indicating that the northeast portion of the Kinleith area is likely one of the later erupted packages, representing the youngest pulses of the Whakamaru ignimbrite. The somewhat narrow geographic range of type

C in the Whakamaru ignimbrite suggests that its eruption is somewhat restricted in both time and space (Figure 6). This final phase of ignimbrite-forming eruptions likely had multiple pulses, as seen in the interbedded morphology of the tephras (Harmon *et al.*, 2024).

The tephra deposits show the chronology of the eruptions, and the ignimbrites provide additional compositional information. Together, this provides a time-integrated view of the magma system, including the melt-dominated magma bodies, magma mush bodies, and the timing of eruptions. While ~40 samples are a tiny minority of the erupted material (>2000 km^3 DRE), the combination of the information derived from them with data from the tephra allows us to finally begin to better constrain the timing of eruption and deposition of the various ignimbrite units.

The Whakamaru Magma System

We demonstrate the presence of two independent magma subsystems that comprise the Whakamaru magma system – one subsystem is responsible for the types A and D magmas, and the other is linked to types B and C magmas. Results for types A, B, and D indicate non-contiguous storage and require that magmas be extracted and subsequently migrated up through the crust away from the mush; for type C, one sample (WHA039J) shows similar storage and extraction pressures, suggesting that contiguous extraction and storage is a possibility for some type C magmas. We show evidence that the Whakamaru magma system is vertically extensive and the glass compositions, storage temperatures, and storage pressures further suggest that the different magma types were likely independent, adjacent, melt-dominated magma bodies (Figures 10 and 11).

The relationship between type B and type C magmas is potentially illuminated by the extraction pressures (Figures 7 and 10). The type C pumice clasts have extraction pressures that partly overlap with type B extraction pressures, but which also extend to shallower pressures that overlap with the type B storage pressures, particularly when considering the storage pressures from both the ignimbrites (this study) and the Kohioawa tephras (Harmon *et al.*, 2024) in combination (Figure 10). It is possible that there was a vertically extensive magma mush system sourcing the type B and type C magmas, where some of the type C magma is extracted from a type B mush at the base of the type B melt-dominated magma body. Since type C was erupted only in the final tephra unit, it is possible that the more evolved, lower Ba and Sr concentrations are a consequence of extraction from the type B magma body following crystallization of two feldspars, as the glass compositions of type B overlap with the whole-rock compositions of type C (Figures 5 and 9). The similarity in the whole-rock and glass compositions, mineral assemblages, and extraction pressures indicates that types B and C are likely related to the same source. However, the slight differences in whole-rock and glass compositions show that the more evolved signature for type C could indicate that it is extracted from type B in a two-part extraction and storage process. This could be both a temporal and/or spatial relationship. This is consistent with observations from the tephra sequences, which show that type C magmas only appear late in the erupted sequence (Harmon *et al.*, 2024). Further work is necessary to better constrain the genetic relationships between type B and type C magmas.

The overlapping storage pressures of the different magma types – both from this study and from Harmon *et al.* (2024) – indicate that the system does not include a single, vertically-zoned magma chamber as proposed by Brown *et al.* (1998). Instead, it is more likely to have consisted of multiple, adjacent, melt-dominated magma bodies. Due to the uncertainties in storage pressure, it is possible, but unlikely, that the magma bodies of different types overlap and mix. Since the Whakamaru and Manunui ignimbrites both contain multiple pumice types, often found in the same outcrop, the compositionally distinct, melt-dominated magma bodies must have coexisted in the crust prior to eruption. Therefore, a single magma body cannot have sourced the Whakamaru group eruptions. Further, the extraction of magma from the two magma subsystems indicates that the Whakamaru system was complex, with multiple sources of melt-dominated magma. Combining the evidence from the ignimbrites (this study) and correlated tephras (Harmon *et al.*, 2024), we conclude that the two subsystems (A+D and B+C) existed for most or all of the eruptive history of the Whakamaru group of eruptions.

The differences in magma chemistry are traced at least to the level of extraction, indicating that the two subsystems simultaneously existed in the crust prior to eruption. This implies that there can be multiple magma subsystems coexisting in the transcrustal magma system. This raises intriguing questions about the origin of the magma subsystems: is each subsystem derived from a different mantle source or are they separated by deeper crustal processes? In either case, the large Whakamaru magmatic system provides evidence for the makeup of transcrustal magmatic systems more broadly.

CONCLUSIONS

In this study, we use matrix-glass and whole-rock compositions of pumice from the Whakamaru group ignimbrites to determine the chemical variability of the magmas erupted, the pressures of magma storage and extraction, and combine evidence from pyroclastic fall material (Harmon *et al.*, 2024) to determine the timing of the eruptions of the different ignimbrites. We find that there are four magma types (types A, B, C, D), confirming the conclusions of Brown *et al.* (1998). Using matrix glass and whole-rock compositional pairs from pumice clasts from the Whakamaru ignimbrite, we find that all magmas were saturated in zircon and that only magma types B and C were saturated in sanidine. The four different types of magma were likely stored in four independent magma bodies laterally juxtaposed to one another in the upper crust (~ 50-150 MPa).

Differences in extraction conditions indicate that the Whakamaru magma system is composed of two magma subsystems - one sourced magma types A + D and the other sourced magma types B + C. The two subsystems have either different magma mush extraction assemblages (orthopyroxene + feldspar for the subsystem that produced types A +D vs. feldspar + quartz for the subsystem that produced types B + C) or different extraction pressures (deeper for the subsystem that produced types A + D vs. shallower for the subsystem that produced types B + C). Evidence from SiO_2 compositions indicates that the first option is more likely and that magmas from the two subsystems were extracted from a constricted crustal range (~ 175-350) in equilibrium with different mineral assemblages (Figure 11). The consistent shallow magma body storage pressures and likely constrained extraction pressures indicate a possible tectonic or structural control on where the melt-dominated magma bodies were extracted and subsequently stored prior to eruption.

There has been substantial debate about the timing of the different Whakamaru group eruptions. Using information from the co-erupted tephras (Harmon *et al.*, 2024), we hypothesize that the Rangitaiki ± Te Whaiti ignimbrites to the east of the Whakamaru caldera erupted first, before the Whakamaru eruptions erupted to the west of the Whakamaru caldera in a later stage. The final stages of the Whakamaru group ignimbrites are the Manunui ignimbrite to the west and the Whakamaru ignimbrite to the northwest, in the Kinleith forest area, where type C magma abounds.

Using petrological and volcanological data from the ignimbrites and the associated tephras, we conclude that the Whakamaru magma system was sourced by two subsystems comprised of both magma mush bodies and melt-dominated magma bodies. These bodies were likely stored at overlapping depths spanning large swaths of the upper crust, although there were likely regions where little to no magma existed. It is only with the combination of data from the spatial distribution of the ignimbrites and the chronology of the tephras that we are able to understand how the Whakamaru group eruptions were extracted, stored, and erupted. Our work adds further evidence that supereruption-forming magmatic systems are characterized by a complex patchwork of laterally juxtaposed melt-dominated magma bodies, and that they can be extracted from magma mush that extends through much of the upper crust – consistent with what has been observed for other mature systems in the Taupō Volcanic Zone and elsewhere in the world.

ACKNOWLEDGEMENTS

We would like to thank Calvin Miller, Mark Ghiorso, and Chad Deering for their assistance throughout the project. Elisabeth Bertolett provided substantial assistance during fieldwork and sampling. Thanks to Mere in Whanganui Bay for access to Whakamaru sampling locations and sharing local knowledge. Steve Self, Fabio Arzilli, and a third reviewer provided thoughtful and helpful reviews that improved the manuscript. We acknowledge the support from National Science Foundation 1714025, EAR-1151337, EAR-1830122 and from Vanderbilt University Discovery Grant.

REFERENCES

Allan, A. S. R., Morgan, D. J., Wilson, C. J. N. & Millet, M. A. (2013). From mush to eruption in centuries: Assembly of the super-sized Oruanui magma body. *Contributions to Mineralogy and Petrology* **166**, 143–164.

Annen, C., Blundy, J. D., Leuthold, J. & Sparks, R. S. J. (2015). Construction and evolution of igneous bodies: Towards an integrated perspective of crustal magmatism. *Lithos*. Elsevier **230**, 206–221.

Bachmann, O. & Bergantz, G. (2008). The magma reservoirs that feed supereruptions. *Elements* **4**, 17–21.

Bachmann, O. & Bergantz, G. W. (2004). On the origin of crystal-poor rhyolites: Extracted from batholithic crystal mushes. *Journal of Petrology* **45**, 1565–1582.

Bachmann, O. & Huber, C. (2016). Silicic magma reservoirs in the Earth's crust. *American Mineralogist*. Walter de Gruyter GmbH **101**, 2377–2404.

Barboni, M. & Schoene, B. (2014). Short eruption window revealed by absolute crystal growth rates in a granitic magma. *Nature Geoscience* **7**, 524–528.

Bégué, F., Deering, C. D., Gravley, D. M., Kennedy, B. M., Chambefort, I., Gualda, G. A. R. & Bachmann, O. (2014a). Extraction, storage and eruption of multiple isolated magma batches in the paired Mamaku and Ohakuri eruption, Taupo Volcanic Zone, New Zealand. *Journal of Petrology* **55**, 1653–1684.

Bégué, F., Gualda, G. A. R., Ghiorso, M. S., Pamukçu, A. S., Kennedy, B. M., Gravley, D. M., Deering, C. D. & Chambefort, I. (2014b). Phase-equilibrium geobarometers for silicic rocks based on rhyolite-MELTS. Part 2: application to Taupo Volcanic Zone rhyolites. *Contributions to Mineralogy and Petrology* **168**, 1–16.

Blundy, J. (2022). Chemical Differentiation by Mineralogical Buffering in Crustal Hot Zones. *Journal of Petrology*. Oxford University Press **63**.

Blundy, J. D. & Cashman, K. V. (2008). Petrologic reconstruction of magmatic system variables and processes. *Reviews in Mineralogy and Geochemistry* **69**, 179–239.

Boehnke, P., Watson, E. B., Trail, D., Harrison, T. M. & Schmitt, A. K. (2013). Zircon saturation re-revisited. *Chemical Geology* **351**, 324–334.

Briggs, N. D. (1976a). Welding and crystallisation zonation in whakamaru ignimbrite, central north island, new zealand. *New Zealand Journal of Geology and Geophysics* **19**, 189–212.

Briggs, N. D. (1976b). Recognition and correlation of subdivisions within the whakamaru ignimbrite, central north island, new zealand. *New Zealand Journal of Geology and Geophysics* **19**, 463–501.

Brown, S. J. A. (1994). Geology and geochemistry of the Whakamaru Group ignimbrites, and associated rhyolite domes, Taupo Volcanic Zone, New Zealand. Christchurch, University of Canterbury.

Brown, S. J. A., Wilson, C. J. N., Cole, J. W. & Wooden, J. L. (1998). The Whakamaru group ignimbrites, Taupo Volcanic Zone, New Zealand: Evidence for reverse tapping of a zoned silicic magmatic system. *Journal of Volcanology and Geothermal Research* **84**, 1–37.

Cashman, K. V & Giordano, G. (2014). Calderas and magma reservoirs. *Journal of Volcanology and Geothermal Research*. Elsevier B.V. **288**, 28–45.

Cashman, K. V., Stephen, R., Sparks, J. & Blundy, J. D. (2017). Vertically extensive and unstable magmatic systems: A unified view of igneous processes. *Science* **355**.

Chakraborty, S. & Dohmen, R. (2022). Diffusion chronometry of volcanic rocks: looking backward and forward. *Bulletin of Volcanology* **84**, 57.

Chamberlain, K. J., Wilson, C. J. N., Wallace, P. J. & Millet, M. A. (2015). Micro-analytical perspectives on the Bishop Tuff and its magma chamber. *Journal of Petrology*. Oxford University Press **56**, 605–640.

Chamberlain, K. J., Wilson, C. J. N., Wooden, J. L., Charlier, B. L. A. & Ireland, T. R. (2014). New perspectives on the Bishop Tuff from zircon textures, ages and trace elements. *Journal of Petrology* **55**, 395–426.

Charlier, B. L. A., Wilson, C. J. N. & Davidson, J. P. (2008). Rapid open-system assembly of a large silicic magma body: Time-resolved evidence from cored plagioclase crystals in the Oruanui eruption deposits, New Zealand. *Contributions to Mineralogy and Petrology* **156**, 799–813.

Cooper, G. F., Morgan, D. J. & Wilson, C. J. N. (2017). Rapid assembly and rejuvenation of a large silicic magmatic system: Insights from mineral diffusive profiles in the Kidnappers and Rocky Hill deposits, New Zealand. *Earth and Planetary Science Letters* **473**, 1–13.

Cooper, G. F., Wilson, C. J. N., Millet, M. A., Baker, J. A. & Smith, E. G. C. (2012). Systematic tapping of independent magma chambers during the 1Ma Kidnappers supereruption. *Earth and Planetary Science Letters* **313–314**, 23–33.

Cooper, K. M. & Kent, A. J. R. (2014). Rapid remobilization of magmatic crystals kept in cold storage. *Nature*. Nature Publishing Group **506**, 480–483.

Deering, C. D., Bachmann, O. & Vogel, T. A. (2011). The Ammonia Tanks Tuff: Erupting a melt-rich rhyolite cap and its remobilized crystal cumulate. *Earth and Planetary Science Letters* **310**, 518–525.

Deering, C. D., Gravley, D. M., Vogel, T. A., Cole, J. W. & Leonard, G. S. (2010). Origins of cold-wet-oxidizing to hot-dry-reducing rhyolite magma cycles and distribution in the Taupo Volcanic Zone, New Zealand. *Contributions to Mineralogy and Petrology* **160**, 609–629.

Downs, D. T., Wilson, C. J. N., Cole, J. W., Rowland, J. V., Calvert, A. T., Leonard, G. S. & Keall, J. M. (2014). Age and eruptive center of the Paeroa Subgroup ignimbrites (Whakamaru Group) within the Taupo Volcanic Zone of New Zealand. *Bulletin of the Geological Society of America* **126**, 1131–1144.

Druitt, T. H., Costa, F., Deloule, E., Dungan, M. & Scaillet, B. (2012). Decadal to monthly timescales of magma transfer and reservoir growth at a caldera volcano. *Nature* **482**, 77–80.

Ewart, A. (1965). Mineralogy and Petrogenesis of the Whakamaru Ignimbrite in the Maraetai area of the Taupo volcanic zone, New Zealand. *New Zealand Journal of Geology and Geophysics* **8**, 611–679.

Ewart, A. & Healy, J. (1966). Te Whaiti ignimbrites at Murupara. In: Thompson, B., Kermode, L. & Ewart, A. (eds) *New Zealand Volcanology*, *Central Volcanic Region*. New Zealand Department of Scientific and Industrial Research Information, 121–125.

Fabbro, G. N., Druitt, T. H. & Costa, F. (2017). Storage and eruption of silicic magma across the transition from dominantly effusive to caldera-forming states at an arc volcano (Santorini, Greece). *Journal of Petrology*. Oxford University Press **58**, 2429–2464.

Foley, M. L., Miller, C. F. & Gualda, G. A. R. (2020). Architecture of a Super-sized Magma Chamber and Remobilization of its Basal Cumulate (Peach Spring Tuff, USA). *Journal of Petrology* **61**.

Ghiorso, M. S. & Gualda, G. A. R. (2015). An H2O–CO2 mixed fluid saturation model compatible with rhyolite-MELTS. *Contributions to Mineralogy and Petrology* **169**, 53.

Ghiorso, M. S., Matthews, S. & Sverjensky, D. A. (2023). MELTS+DEW: Modeling major element+Cl+F+S phase equilibria, redox reactions and elemental partitioning in magmatic-hydrothermal systems. Lyon: Goldschmidt.

Giordano, G. & Caricchi, L. (2022). Determining the State of Activity of Transcrustal Magmatic Systems and Their Volcanoes. *Annual Review of Earth and Planetary Sciences* **50**, 231–259.

Gravley, D. M., Deering, C. D., Leonard, G. S. & Rowland, J. V. (2016). Ignimbrite flare-ups and their drivers: A New Zealand perspective. *Earth-Science Reviews* **162**, 65–82.

Gravley, D. M., Wilson, C. J. N., Leonard, G. S. & Cole, J. W. (2007). Double trouble: Paired ignimbrite eruptions and collateral subsidence in the Taupo Volcanic Zone, New Zealand. *Bulletin of the Geological Society of America* **119**, 18–30.

Grindley, G. (1960). Geological Map of New Zealand 1:250,000. *NZ Department of Scientific and Industrial Research*. Wellington, New Zealand.

Gualda, G. A. R. & Ghiorso, M. S. (2013a). Low-Pressure Origin of High-Silica Rhyolites and Granites. *The Journal of Geology* **121**, 537–545.

Gualda, G. A. R. & Ghiorso, M. S. (2013b). The Bishop Tuff giant magma body: an alternative to the Standard Model. *Contributions to Mineralogy and Petrology* **166**, 755–775.

Gualda, G. A. R. & Ghiorso, M. S. (2014). Phase-equilibrium geobarometers for silicic rocks based on rhyolite-MELTS. Part 1: Principles, procedures, and evaluation of the method. *Contributions to Mineralogy and Petrology* **168**, 1–17.

Gualda, G. A. R., Ghiorso, M. S., Hurst, A. A., Allen, M. C. & Bradshaw, R. W. (2022). A complex patchwork of magma bodies that fed the Bishop Tuff supereruption (Long Valley Caldera, CA, United States): Evidence from matrix glass major and trace-element compositions. *Frontiers in Earth Science* **10**.

Gualda, G. A. R., Gravley, D. M., Conner, M., Hollmann, B., Pamukçu, A. S., Bégué, F., Ghiorso, M. S. & Deering, C. D. (2018). Climbing the crustal ladder: Magma storage-depth evolution during a volcanic flare-up. *Science Advances* **4**, eaap7567.

Gualda, G. A. R., Gravley, D. M., Deering, C. D. & Ghiorso, M. S. (2019). Magma extraction pressures and the architecture of volcanic plumbing systems. *Earth and Planetary Science Letters*. Elsevier B.V. **522**, 118–124.

Gualda, G. A. R. & Sutton, S. R. (2016). The year leading to a supereruption. *PLoS ONE* **11**, 1–18.

Hansteen, T. H. & Klügel, A. (2008). Fluid inclusion thermobarometry as a tracer for magmatic processes. *Reviews in Mineralogy and Geochemistry* **69**, 143–177.

Harmon, L. J., Cowlyn, J., Gualda, G. A. R. & Ghiorso, M. S. (2018). Phase-equilibrium geobarometers for silicic rocks based on rhyolite-MELTS. Part 4: Plagioclase, orthopyroxene, clinopyroxene, glass geobarometer, and application to Mt. Ruapehu, New Zealand. *Contributions to Mineralogy and Petrology* **173**, 7.

Harmon, L. J., Gualda, G. A. R., Gravley, D. M., Smithies, S. L. & Deering, C. D. (2024). The Whakamaru magmatic system (Taupō Volcanic Zone, New Zealand), part 1: Evidence from tephra deposits for the eruption of multiple magma types through time. *Journal of Volcanology and Geothermal Research*. Elsevier **445**, 107966.

Hildreth, W. (1979). The Bishop Tuff: Evidence for the origin of compositional zonation in silicic magma chambers. *Geological Society of America* **Special Paper 180**.

Hildreth, W. (2004). Volcanological perspectives on Long Valley, Mammoth Mountain, and Mono Craters: Several contiguous but discrete systems. *Journal of Volcanology and Geothermal Research* **136**, 169–198.

Hildreth, W. & Wilson, C. J. N. (2007). Compositional zoning of the bishop tuff. *Journal of Petrology* **48**, 951–999.

Hilley, G. E. (ed.), Brodsky, E. E., Roman, D., Shillington, D. J., Brudzinski, M., Behn, M., Tobin, H. & the SZ4D RCN (2022). *SZ4D Implementation Plan.* .

Houghton, B. F., Wilson, C. J. N., McWilliams, M. O., Lanphere, M. A., Weaver, S. D., Briggs, R. M. & Pringle, M. S. (1995). Chronology and dynamics of a large silicic magmatic system: Central Taupo Volcanic Zone, New Zealand. *Geology* **23**, 13–16.

Iacovino, K., Matthews, S., Wieser, P. E., Moore, G. M. & Bégué, F. (2021). VESIcal Part I: An Open-Source Thermodynamic Model Engine for Mixed Volatile (H2O-CO2) Solubility in Silicate Melts. *Earth and Space Science*. John Wiley and Sons Inc **8**.

Karakas, O., Degruyter, W., Bachmann, O. & Dufek, J. (2017). Lifetime and size of shallow magma bodies controlled by crustal-scale magmatism. *Nature Geoscience* **10**, 446–450.

Kelley, K. A. & Cottrell, E. (2009). Water and the Oxidation State of Subduction Zone Magmas. *Science* **325**, 605–607.

Leonard, G. S., Begg, J. G. & Wilson, C. J. N. (2010). Geology of the Rotorua area. Lower Hutt, New Zealand: GNS Science.

Manning, D. A. (1995). Late Pleistocene Tephrostratigraphy of the Eastern Bay of Plenty Region, New Zealand. Wellington, Victoria University.

Manning, D. A. (1996). Middle-late Pleistocene tephrostratigraphy of the eastern Bay of Plenty, New Zealand. *Quaternary International* **34–36**, 3–12.

Martin, R. C. (1961). Stratigraphy and structural outline of the Taupo Volcanic Zone. *New Zealand Journal of Geology and Geophysics* **4**, 449–478.

Martin, R. C. (1965). Lithology and eruptive history of the Whakamaru ignimbrites in the Maraetai area of the Taupo volcanic zone, New Zealand. *New Zealand Journal of Geology and Geophysics* **8**, 680–705.

Matthews, N. E. (2011). Magma chamber assembly and dynamics of a supervolcano: Whakamaru, Taupo Volcanic Zone, New Zealand. Oxford, University of Oxford.

Matthews, N. E., Smith, V. C., Costa, A., Durant, A. J., Pyle, D. M. & Pearce, N. J. G. (2012). Ultra-distal tephra deposits from super-eruptions: Examples from Toba, Indonesia and Taupo Volcanic Zone, New Zealand. *Quaternary International* **258**, 54–79.

McCanta, M. C., Dyar, M. D., Rutherford, M. J. & Delaney, J. S. (2004). Iron partitioning between basaltic melts and clinopyroxene as a function of oxygen fugacity. *American Mineralogist* **89**, 1685–1693.

Moore, G., Vennemann, T. & Carmichael, I. S. E. (1998). An empirical model for the solubility of H2O in magmas to 3 kilobars. *American Mineralogist*. Mineralogical Society of America **83**, 36–42.

Pamukçu, A. S., Carley, T. L., Gualda, G. A. R., Miller, C. F. & Ferguson, C. A. (2013). The evolution of the peach spring giant magma body: Evidence from accessory mineraltextures and compositions, bulk pumice and glass geochemistry, and rhyolite-MELTS modeling. *Journal of Petrology* **54**, 1109–1148.

Pamukçu, A. S., Gualda, G. A. R., Bégué, F. & Gravley, D. M. (2015a). NOT Melt inclusion shapes: Timekeepers of short-lived giant magma bodies. *Geology* **43**, 947–950.

Pamukçu, A. S., Gualda, G. A. R., Ghiorso, M. S., Miller, C. F. & McCracken, R. G. (2015b). Phase-equilibrium geobarometers for silicic rocks based on rhyolite-MELTS—Part 3: Application to the Peach Spring Tuff (Arizona–California–Nevada, USA). *Contributions to Mineralogy and Petrology* **169**, 1–17.

Pamukçu, A. S., Gualda, G. A. R. & Gravley, D. M. (2021). Rhyolite-MELTS and the storage and extraction of large-volume crystal-poor rhyolitic melts at the Taupō Volcanic Center: a reply to Wilson et al. (2021). *Contributions to Mineralogy and Petrology*. Springer Science and Business Media Deutschland GmbH **176**.

Papale, P., Moretti, R. & Barbato, D. (2006). The compositional dependence of the saturation surface of H2O + CO2 fluids in silicate melts. *Chemical Geology*. Elsevier **229**, 78–95.

Pearce, N. J. G., Westgate, J. A., Gualda, G. A. R., Gatti, E. & Muhammad, R. F. (2020). Tephra glass chemistry provides storage and discharge details of five magma reservoirs which fed the 75 ka Youngest Toba Tuff eruption, northern Sumatra. *Journal of Quaternary Science*. John Wiley and Sons Ltd **35**, 256–271.

Pelullo, C., Iovine, R. S., Arienzo, I., Di Renzo, V., Pappalardo, L., Petrosino, P. & D’antonio, M. (2022). Mineral-Melt Equilibria and Geothermobarometry of Campi Flegrei Magmas: Inferences for Magma Storage Conditions. *Minerals*. MDPI **12**.

Pitcher, B. W., Gualda, G. A. R. & Hasegawa, T. (2021). Repetitive Duality of Rhyolite Compositions, Timescales, and Storage and Extraction Conditions for Pleistocene Caldera-forming Eruptions, Hokkaido, Japan. *Journal of Petrology*. Oxford University Press **62**, egaa106.

Putirka, K. D. (2008). Thermometers and Barometers for Volcanic Systems. *Reviews in Mineralogy and Geochemistry* **69**, 61–120.

Reid, M. R. & Vazquez, J. A. (2017). Fitful and protracted magma assembly leading to a giant eruption, Youngest Toba Tuff, Indonesia. *Geochemistry Geophysics Geosystems* **18**, 156–177.

Ridolfi, F., Renzulli, A. & Puerini, M. (2010). Stability and chemical equilibrium of amphibole in calc-alkaline magmas: An overview, new thermobarometric formulations and application to subduction-related volcanoes. *Contributions to Mineralogy and Petrology* **160**, 45–66.

Shamloo, H. I. & Till, C. B. (2019). Decadal transition from quiescence to supereruption: petrologic investigation of the Lava Creek Tuff, Yellowstone Caldera, WY. *Contributions to Mineralogy and Petrology*. Springer Verlag **174**.

Simon, J. I. & Reid, M. R. (2005). The pace of rhyolite differentiation and storage in an "archetypical" silicic magma system, Long Valley, California. *Earth and Planetary Science Letters* **235**, 123–140.

Smithies, S. L., Harmon, L. J., Allen, S. M., Gravley, D. M. & Gualda, G. A. R. (2023). Following magma: The pathway of silicic magmas from extraction to storage during an ignimbrite flare-up, Taupō Volcanic Zone, New Zealand. *Earth and Planetary Science Letters*. Elsevier B.V. **607**, 118053.

Sparks, R. S. J., Annen, C., Blundy, J. D., Cashman, K. V., Rust, A. C. & Jackson, M. D. (2019). Formation and dynamics of magma reservoirs. *Philosophical Transactions of the Royal Society A: Mathematical, Physical and Engineering Sciences* **377**.

Stagpoole, V., Miller, C., Caratori Tontini, F., Brakenrig, T. & Macdonald, N. (2021). A two million-year history of rifting and caldera volcanism imprinted in new gravity anomaly compilation of the Taupō Volcanic Zone, New Zealand. *New Zealand Journal of Geology and Geophysics*. Taylor & Francis **64**, 358–371.

Swallow, E. J., Wilson, C. J. N., Myers, M. L., Wallace, P. J., Collins, K. S. & Smith, E. G. C. (2018). Evacuation of multiple magma bodies and the onset of caldera collapse in a supereruption, captured in glass and mineral compositions. *Contributions to Mineralogy and Petrology*. Springer Berlin Heidelberg **173**, 1–22.

Ulmer, P., Kaegi, R. & Müntener, O. (2018). Experimentally derived intermediate to silica-rich arc magmas by fractional and equilibrium crystallization at 1·0 GPa: An evaluation of phase relationships, compositions, liquid lines of descent and oxygen fugacity. *Journal of Petrology*. Oxford University Press **59**, 11–58.

Waters, L. E. & Lange, R. A. (2015). An updated calibration of the plagioclase-liquid hygrometer-thermometer applicable to basalts through rhyolites. *American Mineralogist*. Walter de Gruyter GmbH **100**, 2172–2184.

Watson, E. B. & Harrison, T. M. (1983). Zircon saturation revisited: temperature and composition effects in a variety of crustal magma types. *Earth and Planetary Science Letters* **64**, 295–304.

Weinberg, R. F., Vernon, R. H. & Schmeling, H. (2021). Processes in mushes and their role in the differentiation of granitic rocks. *Earth-Science Reviews*. Elsevier B.V.

Wieser, P. E., Iacovino, K., Matthews, S., Moore, G. & Allison, C. M. (2022). VESIcal: 2. A Critical Approach to Volatile Solubility Modeling Using an Open-Source Python3 Engine. *Earth and Space Science*. John Wiley and Sons Inc **9**, e2021EA001932.

Wilson, C. J. N., Gravley, D. M., Leonard, G. S. & Rowland, J. V. (2009). Volcanism in the central Taupo Volcanic Zone, New Zealand: tempo styles and controls. *Special Publications of IAVCEI* **2**, 225–247.

Wilson, C. J. N., Houghton, B. F. & Lloyd, E. F. (1986). Volcanic history and evolution of the Maroa-Taupo area. In: Smith, I. E. M. (ed.) *Late Cenozioc Volcanism in New Zealand*. Wellington: The Royal Society of New Zealand Bulletin, 194–223.

Wilson, C. J. N., Houghton, B. F., McWilliams, M. O., Lanphere, M. A., Weaver, S. D. & Briggs, R. M. (1995). Volcanic and structural evolution of Taupo Volcanic Zone, New Zealand: a review. *Journal of Volcanology and Geothermal Research* **68**, 1–28.

Wilson, C. J. N., Rogan, A. M., Smith, I. E. M., Northey, D. J., Nairn, I. A. & Houghton, B. F. (1984). Caldera volcanoes of the Taupo volcanic zone, New Zealand. *Journal of Geophysical Research* **89**, 8463–8484.

Wotzlaw, J.-F., Bindeman, I. N., Watts, K. E., Schmitt, A. K., Caricchi, L. & Schaltegger, U. (2014). Linking rapid magma reservoir assembly and eruption trigger mechanisms at evolved Yellowstone-type supervolcanoes. *Geology* **42**, 807–810.

SUPPLEMENTARY MATERIAL

1. Description of the four ignimbrites (Whakamaru, Rangitaiki, Manunui, and Te Whaiti) from the literature, predominantly after Brown *et al.* (1998) and references therein.
2. Description of the four compositional types of rhyolite pumice (types A, B, C, and D) after Brown *et al.* (1998), Brown (1994), Matthews (2011), and Saunders *et al.* (2010).
3. Whole-rock compositional data and extraction pressure geobarometry results from pumice clasts from the Whakamaru group ignimbrites
4. Matrix glass compositional data, geothermometry results, and storage pressure geobarometry results from pumice clasts from the Whakamaru group ignimbrites
5. Sample metadata, including sampling coordinates and analyses performed
6. USGS RGM standard major-element data for SEM-EDS